Hydrophobic Mismatch Influencing the Structure-Function Relationship of the Reaction Center from Photosynthetic Bacterium *Rhodobacter sphaeroides*

Kai Tang

A Thesis

in

the Department

of

Chemistry & Biochemistry

For the Degree of Master of Science at
Concordia University
Montreal, Quebec, Canada

September 2008

Library and
Archives Canada

Published Heritage
Branch

395 Wellington Street
Ottawa ON K1A 0N4
Canada

Bibliothèque et
Archives Canada

Direction du
Patrimoine de l'édition

395, rue Wellington
Ottawa ON K1A 0N4
Canada

Your file Votre référence
ISBN: 978-0-494-45715-3
Our file Notre référence
ISBN: 978-0-494-45715-3

Abstract

Hydrophobic Mismatch Influencing the Structure-Function Relationship of the Reaction Center from Photosynthetic Bacterium *Rhodobacter sphaeroides*

Kai Tang

The photosynthetic organisms consist a cluster of membrane bound protein-pigment complexes, which utilize absorbed photons to drive electron transfer reactions to convert light energy into chemical energy. In the photosynthetic bacterial reaction center from *Rhodobacter sphaeroides*, light induces a transfer of an electron from the primary electron donor, a special pair of two bacteriochorophylls forming a dimer, through a series of intermediate electron acceptors and a primary quinone Q_A, to a reversibly-bound quinone Q_B. Reaction centers from *Rhodobacter sphaeroides* have been reconstituted into various liposomes, with varying fatty acid chain lengths from C_{12} to C_{18}, resulting in different hydrophobic thicknesses of the lipid bilayer. Compensations are expected both from the lipid and the protein if the hydrophobic thicknesses are not matched. Lipid-protein interactions were explored and identified due to this hydrophobic mismatch by studying the phase behavior of the lipid and probing the function of the protein. The optimal thickness for the membrane, using saturated phospholipids to incorporate the bacterial reaction center, was found to be equivalent to a carbon length of C_{14}. Prolonged illumination induced conformational rearrangements in the protein structure. Lipid environment, acidic pH, long illumination, and low temperature favored the formation of the long-lived charge separated state. This light-adapted conformation had a lifetime up to 8.9 hours, which is three million times as much as the lifetime of the dark-adapted charge separated state induced by flash excitations.

Acknowledgement

I wish to thank my supervisor, Dr. Laszlo Kalman, for the valuable help throughout this project and for the careful reading of the manuscript. I am grateful to Drs. Joanne Turnbull and Cameron Skinner for helpful discussions and for continuous advices. Colleague Sasmit Deshmukh is thanked for the measurements in detergent.

Table of contents

List of Figures

List of Tables and Schemes

Abbreviations

BChl	Bacteriochlorophyll monomer
BΦ	Bacteriopheophytin
BRC	Bacterial Reaction Center
DLPC	1,2-Dilauroyl-*sn*-Glycero-3-Phosphocholine, $C_{12:0}$
DMPC	1,2-Dimyristoyl-*sn*-Glycero-3-Phosphocholine, $C_{14:0}$
DPPC	1,2-Dipamytoyl-*sn*-Glycero-3-Phosphocholine, $C_{16:0}$
DSPC	1,2-Distearoyl-*sn*-Glycero-3-Phosphocholine, $C_{18:0}$
DOPC	1,2-Dioleoyl-*sn*-Glycero-3-Phosphocholine, $C_{18:1}$
DPH:	1,6-diphenylhexatriene
DPI	Dual polarization interferometry
EDTA	Ethylenediaminetetraacetic acid
I	Intermediate electron acceptors of BRC
LDAO	Lauryldimethylamine-oxide
LFP	Laser flash photolysis
P	Special pair of bacteriochlorophylls, primary electron donor of BRC
PS II	Photosystem II
Q_A	Quinone A, primary electron acceptor of BRC
Q_B	Quinone B, secondary electron acceptor of BRC
SAS	Solvent accessible surface
TEN	Tris-HCl, EDTA, NaCl
THF	Tetrahydrofuran
TLE	Tris-HCl, LDAO, EDTA

Introduction

1.1 Introduction of photosynthesis

Photosynthesis takes place in green plants, phytoplankton, algae, cyanobacteria , and photosynthetic bacteria where light energy is converted into chemical energy. There are two types of photosynthesis, oxygenic and anoxygenic. Both oxygenic and anoxygenic photosynthetic organisms consist a cluster of membrane-bound protein-pigment complexes, photosystem II (PS II) and bacterial reaction center (BRC), respectively. These complexes utilize absorbed photons to drive electron transfer reactions to convert light energy into chemical energy. Even though both complexes transfer electrons and protons across the membrane in analogous manners, they utilize different secondary electron donors.

In PS II, the primary donor (P680), with a very high oxidation-reduction potential, is reduced by a tyrosine residue, a secondary electron donor that couples the electron transfer to the proton transfer. A tetranuclear Mn cluster that is able to collect four electron equivalents becomes oxidized as light excitation continues. Two water molecules are oxidized into molecular oxygen. In the BRC, exogenous cytochromes with much lower potentials act as secondary electron donors and reduce the primary donor (P) (Ke 2001, Kalman et al., 2008). Because of structural and functional similarities, the well characterized BRC has served as a model for the evolutionarily-related PS II for many years.

1.2 Structure of photosynthetic bacterial reaction center

The three-dimensional structure of *Rhodobacter (Rb) sphaeroides* bacterial reaction center (BRC, Fig.1a), typical as photosynthetic purple bacterium, has been characterized by the X-ray diffraction method, which has helped to elucidate the structure-function relationship (Allen et al., 1987). With 848 amino acid residues and a molecular weight of around 100 kDa (kg/mol), the *Rb. sphaeroides* reaction center contains L-, M- and H subunits, with 5, 5 and 1 transmembrane α-helices, respectively. Several cofactors were found to be associated with the L- and M- subunits (Fig.1b), including one bacteriochlorophyll dimer (P), two bacteriochlorophyll monomers ($BChl_a$ and $BChl_b$), two bacteriopheophytins ($B\Phi_a$ and $B\Phi_b$), two ubiquinones (Q_A and Q_B) and a non-heme iron. The H-subunit contains no cofactors. However, its cytoplasmic domain is suggested to be related to the electron transfer between Q_A and Q_B and the delivery of the protons to Q_B (Ke 2001).

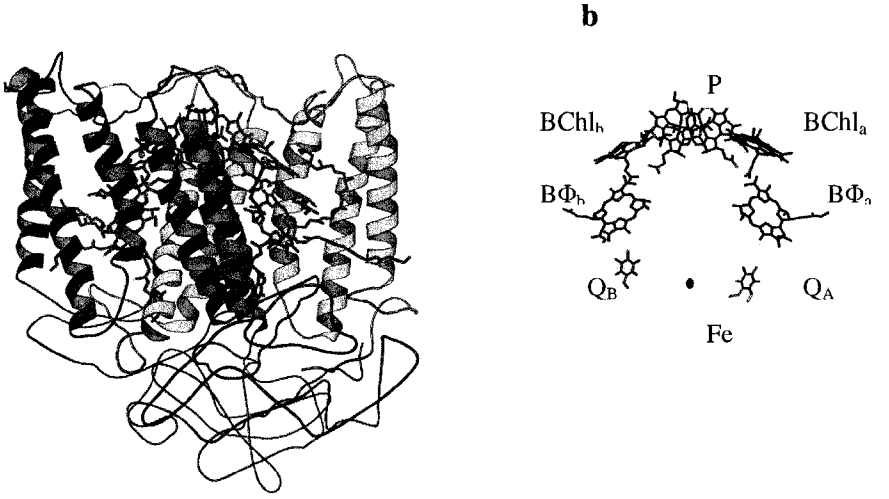

Figure 1. Three-dimensional structure of the photosynthetic reaction center from *Rb. sphaeroides*. (a) Ribbon structure of the isolated BRC, L-subunit (yellow), M-subunit (Blue), H-subunit (Green). (b) Cofactor structures of the BRC. Shaded areas are naturally embedded in the membranes. Modified from Protein Data Bank code 1AIJ

1.3 Electron transfer reactions in BRC

Light induces a transfer of an electron from the primary electron donor, a special pair of two bacteriochlorophylls forming a dimer, through a series of intermediate electron acceptors (I) including a bactriochlorophyll monomer, a bacteriopheophytin and a primary quinone Q_A, to a reversibly-bound quinone Q_B (Fig.2a). After the oxidized P^+ is reduced by the secondary donor cytochrome c_2 (cyt c_2), it can be excited again, resulting in the transfer of a second electron. Q_B finally accepts two electrons and gets fully reduced while taking up two protons as well (Ke 2001).

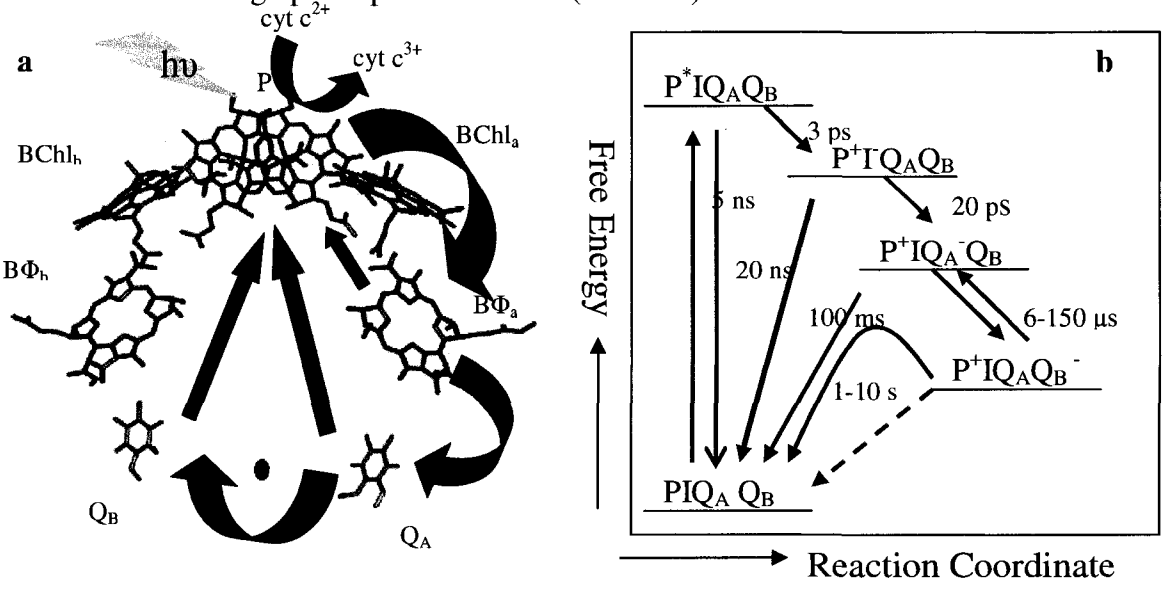

Figure 2. Light-induced electron transfer process in photosynthetic bacterial reaction centers. (a) Electron transfers pathway. (b) Energetic states during the electron transfer process. Green arrows show the forward electron transfer while red arrows show the charge recombination processes.

Figure 2b shows the free energy levels of different states during the electron transfer process. The forward electron transfer is favorable since it is orders of magnitude faster than the charge recombination, resulting in a close to unity quantum yield for charge separation. For example, electron transfer from Q_A^- to Q_B takes place within 100 μs while

the charge recombination from $P^+Q_A^-$ to PQ_A requires 100 ms. Even though the cofactor structure of BRC appears to be highly symmetric, electron transfer only occurs though the "A branch" to Q_B (shown as green arrows in Fig.2A). This is due to the fact that $P^+BChl_b^-$ has a higher energy level than $PBChl_b$. The electron transfer from Q_A^- to Q_B is attributed to the different red-ox properties of the two ubiquinones, which are caused by amino acid domain surroundings of Q_A and Q_B, respectively. Moreover, the non-heme iron is closer to Q_B by about 2Å which also lowers the energy of Q_B^- (Ke 2001).

1.4 Photosynthetic electron transfer cycle in the membrane

The complete photosynthetic electron transfer cycle in the membrane of photosynthetic bacterium *Rb. sphaeroides* is shown schematically in Figure 3. Light induces a transfer of an electron from the primary electron donor to a reversibly-bound quinone Q_B (discussed in Section *1.3*). Q_B is fully reduced by two electrons while taking up two protons from the cytoplasmic side. The reduced quinol Q_BH_2 is released in the membrane and oxidized by cytochrome bc_1 complex (cyt bc_1). There is a quinone pool in the membrane between cyt bc_1 and BRC, which can exchange the reduced Q_BH_2 with quinones. Protons are released at the periplasmic side through cyt bc_1, generating a proton electrochemical gradient. This transmembrane proton gradient serves as the driving force for ATP synthesis. Cyt c_2 acts as a secondary electron donor that carries an electron from cyt bc_1 to the oxidized primary donor P^+ by the heme iron.

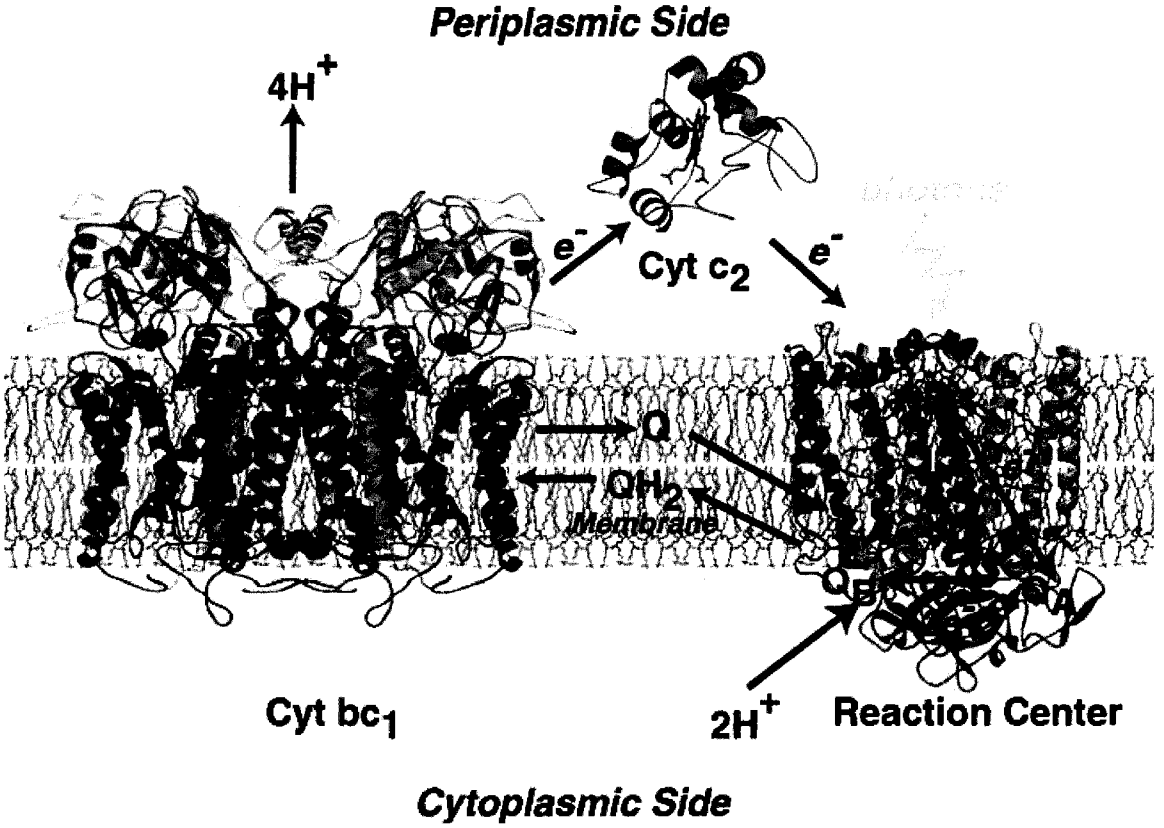

Figure 3. Complete photosynthetic electron transfer cycle in the membrane of the photosynthetic bacterium *Rb. sphaeroides*. Light induces a transfer of an electron from the primary electron donor, a special pair of bacteriochorophylls forming a dimer, to a reversibly-bound quinone Q_B. The fully-reduced quinone is released and re-oxidized by cytochrome bc_1 complex. Cytochrome c_2 acts as a secondary electron donor to complete the electron transfer cycle. The transmembrane proton gradient serves as the driving force for ATP synthesis. Figure is taken from (Axelrod & Okamura 2005).

1.5 Comparison of natural membrane environment and detergent environment

Isolated BRCs are not water soluble due to their large hydrophobic regions. The solubilization is achieved by using detergents, which form a toroidal shielded micelle structure around the hydrophobic region normally embedded in the membrane (Roth et al., 1991). Most structural and functional studies of BRCs have been done in a detergent environment, because the purified BRC is lack of spectroscopic overlaps arising from the

antenna complexes as well as the cyt bc_1 complex and the scattering caused by the membrane lipids making it ideal for spectroscopic studies.

The hydrophobic thickness of the detergent micelle is about 23Å, determined from neutron scattering studies, which is about 5Å thinner than that of the hydrophobic transmembrane helices (Roth et al., 2001). Furthermore, the detergent molecules are very likely oriented with their alkyl chains pointing towards the hydrophobic regions of BRC minimizing the solvent accessible surface (SAS), while the hydrophilic head groups are located at the external surface of the detergent phase (Fig.4a and 4b). Localization of detergent around the photosynthetic reaction center from *Rb. sphaeroides* has been determined by low-resolution neutron diffraction experiments (Fig.4c). The question arises as to how good a representation for membrane proteins such as BRCs is the detergent environment for the natural membrane (Fig.4d). There are more and more indications that the kinetics and thermodynamics of the electron transfer reactions in BRCs have different features in chromatophores (natural membrane fragments), which resemble the conditions *in vivo*. For example, the $P^+Q_B^- \rightarrow PQ_B$ has 1 s lifetime in detergent micelles while it is around 10 s in chromatophores (Trotta el al., 2002).

The lipid composition of cell membrane of purple bacterium *Rhodobacter sphaeroides* is complex, containing a variety of phospholipids, phosphatidylcholine, phosphatidylethanolamin, phosphatidylglycerol and other lipids depending on specific growth conditions, in particular the oxygen level (Camaras-Artigas et al., 2002). The lipid environment is known to have a significant influence on the morphology of the cell

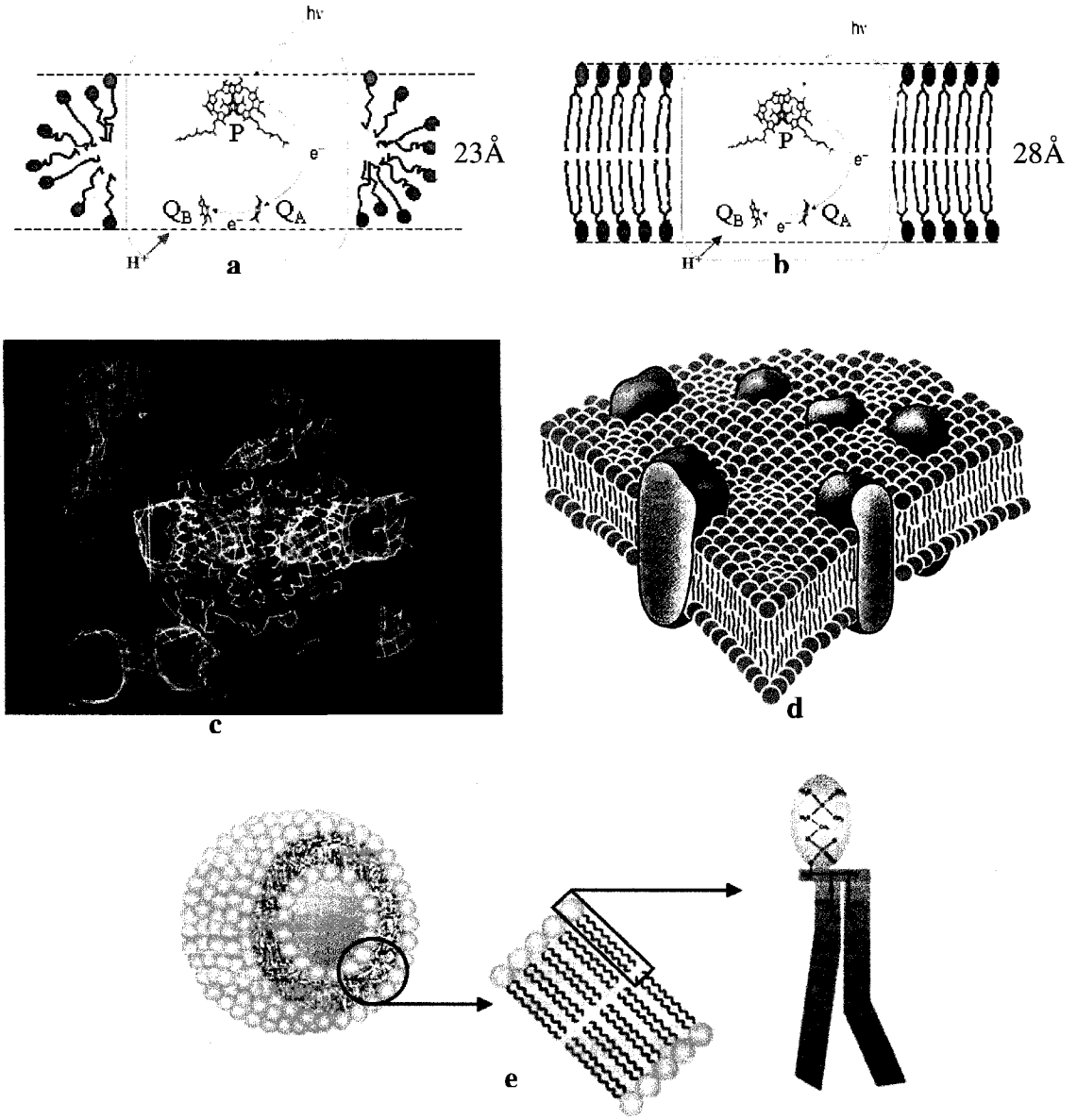

Figure 4. Comparison between natural membrane environment and substituted detergent micelles of reaction centers from *Rb. sphaeroides.* (a) Detergent micelle surrounding BRC. (b) Lipid bilayers from natural membranes surrounding BRC. (c) BRC with its detergent-phase ring structure using neutron diffraction experiments (Roth et al., 1991). (d) Fluid mosaic model of membrane proteins in natural membrane environment, proteins (black) are imbedded in the lipid bilayers (pink as head group, green as fatty acid chain). (e) Artificial liposomes made of phospholipids. Lipids tend to form a spherical liposomes structure of minimize the solvent accessible surface.

membrane, but whether it can affect the photosynthetic energy transfer process remains an outstanding question. A promising approach is to reconstitute the BRCs into proteoliposomes (Fig.4e) with varying fatty acid chain lengths, resulting in different hydrophobic thicknesses of the lipid bilayers. These artificial liposomes are used to mimic the natural membrane environment and to study the structure-function relationship.

1.6 Hydrophobic mismatch

It is obligatory that the hydrophobic thickness of the protein should be equal to the hydrophobic thickness of the membrane. If the hydrophobic region of the membrane protein is thicker or thinner than the hydrocarbon fatty acid chain length of the lipid bilayer, a tension is created to minimize the SAS. This hydrophobic mismatch tension can be resolved in two major ways: either the lipid bilayer should deform to match the hydrophobic thickness of the protein (Fig.5a) or the protein should adjust to match the bilayer (Fig.5b).

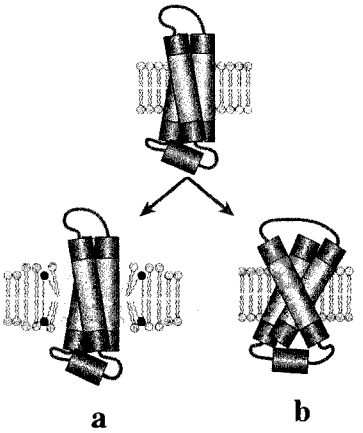

Figure 5. Hydrophobic mismatch. It is required that the hydrophobic thickness of the lipid membrane (Brown) should match with the hydrophobic thickness of the protein (Blue). If this condition is not met, compensation should be made by both the lipid (a) and the protein (b) to minimize this mismatch. Figure is taken from (Bowie 2005).

1.6.1 Lipid response to hydrophobic mismatch

In response to the hydrophobic mismatch, the lipid near the region where hydrophobic mismatch occurs will be disordered. Under optimal circumstances that the hydrophobic thickness of the lipid bilayer is equal to the hydrophobic thickness of the protein, no disordering from the lipid occurs (Fig.6b). If the hydrophobic thickness of the lipid bilayer is shorter than that of the membrane protein, a certain range of the lipids near the protein have to stretch to minimize the mismatch (Fig.6a). On the other hand, the lipids near the protein must compress if the hydrophobic thickness of the lipid bilayer is longer than that of the protein (Fig.6c).

Lipid response to the hydrophobic mismatch can be studied by the phase transition of the lipids. Lipids have two phases depending on what temperature they are at, a gel phase of which the hydrocarbon chains are fully extended and closely packed and a liquid crystalline phase of which the hydrocarbon chains are randomly oriented and fluidic. The phase transition temperature is defined as the temperature required to induce a change in the lipid physical state from the ordered gel phase, to the disordered liquid crystalline phase. By incorporating the BRCs into lipid bilayers, the phase transition temperature should not change if the lipid-protein interaction does not generate a hydrophobic mismatch. The shift in the midpoint transition temperature (ΔT) is defined as the difference between the phase transition temperature with BRCs and the phase transition temperature of the empty liposomes (Sperotto & Mouritsen 1988). The direction and the extent of the change in the phase transition temperature are closely related to the hydrophobic interactions between the lipid and the protein.

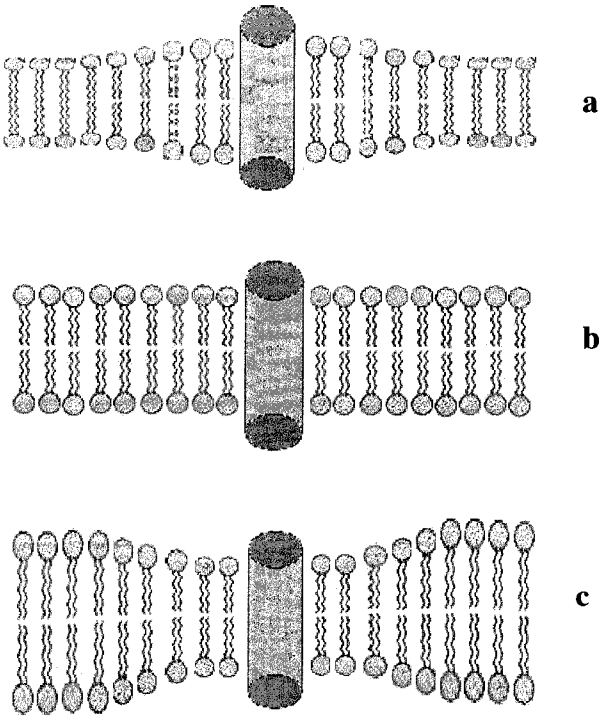

Figure 6. Compensation for the hydrophobic mismatch from the lipid. Ideal case that the hydrophobic thickness of the lipid (brown tails) is equal to hydrophobic thickness of the protein (blue) is shown in panel b, which does not require any compensation. If the fatty acid chain length is different from the hydrophobic thickness of the protein, the lipid near BRC should either stretch (5a) or compress (5c).

1.6.2 Protein compensation in response to hydrophobic mismatch

Proteins make conformational rearrangements to compensate for the hydrophobic mismatch as well. A change in helix tilt with respect to the hydrophobic mismatch (Fig.7a) has been demonstrated in model transmembrane helical proteins. Aggregation (Fig.7b) of proteins in response to the hydrophobic mismatch was a further consideration, which finally resulted in the loss of the function of the proteins (Sanderson 2005). Since the tilt angle is limited, the proteins have to aggregate in response to the hydrophobic mismatch that cannot be completely compensated for by tilting. In BRCs from *Rb. sphaeroides*, the crystal structure revealed that the helices are not vertically aligned in the

membrane, instead they seem to tilt to adjust to the hydrophobic mismatch generated by the detergent belt being thinner than the hydrophobic length of the transmembrane helices (see Figure 1).

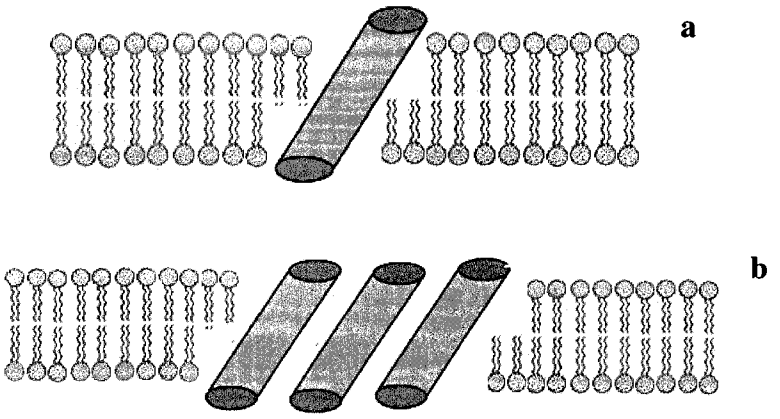

Figure 7. Compensation for the hydrophobic mismatch from the protein. The protein can either (a) tilt the angle of its transmembrane helices, or (b) aggregate to minimize the extent of the mismatch.

In the case of BRC, protein response to the hydrophobic mismatch can be studied by the conformational rearrangements during electron transfer reactions. Under physiological conditions, the charge recombination of the reaction center from *Rb. sphaeroides* occurs in 100 ms and 1 s time scale from the primary and secondary reduced quinones, respectively (see Figure 2b). The electron transfer is accompanied by conformational changes and proton uptake reactions of the BRC. Upon continuous illumination, however, the recovery can be much longer, due to the formation of an altered light-adapted conformation. The formation of the long-lived state does not depend on the presence of the secondary quinone since the light-dark absorption difference spectrum of the long-lived state is very similar to that of the normal $P^+Q_A^-$ or $P^+Q_B^-$ spectrum (Mourik et al., 2001). These indicate a fully-reversible conformational rearrangement of the

protein induced by the electric field of the charge-separated state.

On the cytoplasmic side, two binding conformations for the Q_B head group were found due to the presence of a charge upon illumination (Stowell et al., 1997). The first binding position is proximal to the non-heme iron and symmetrical to that of the Q_A quinone head group, which was seen with the BRC crystals frozen to cryogenic temperatures under continuous illumination. The second, distal binding position was identified when the BRC crystals were frozen in the dark. On the periplasmic side of the BRC, two distinct conformations of P^+ were reported depending on the detergent and the temperature (Muh et al., 1997). The two distinct conformations of the BRC were found to be dependent on the pH, red-ox potential of P/P^+ and illumination conditions.

The lipid environment also appears to play a significant role in the energetic stabilization of the charge separated state. A large stabilizing effect on the charge separated state induced by anionic phospholipids was reported (Agostiano et al., 2005). The lifetime and the relative yield of the long-lived state were increased at low pH (Kalman & Maroti 1997). By incorporating BRCs into various liposomes with different fatty acid chain lengths, protein response to the hydrophobic mismatch can be studied through electron transfer reactions.

1.7 Research Perspectives

Artificial membranes provide a better approximation than the detergent micelle environment to explore the structure-function relationship of the BRCs because they

represent a milieu that closely resembles the conditions *in vivo.* By systematically optimizing the membrane environment, our ultimate goal is to develop an artificial membrane system that maximizes the function of the BRC. Since only a few studies have been done in the lipid environment, it is crucial to understand the structure-function relationship between the BRCs and different lipid environments. This project is one step in this direction.

Photosynthetic reaction centers from *Rb. sphaeroides* have been reconstituted into various liposomes, with varying fatty acid chain lengths from C_{12} to C_{18}, resulting in different hydrophobic thicknesses of the lipid bilayers. Lipid-protein interactions were explored and identified due to this hydrophobic mismatch by studying the phase behavior of the lipid and probing the function of the BRC. Two models have been used to quantitatively characterize the hydrophobic mismatch. By systematically changing the environmental factors, such as liposomes with different hydrophobic thicknesses, pH, temperature, and illumination conditions, a long-lived charge separated state that significantly altered the energetics of the electron transfer rate was generated.

2 Materials and Methods

2.1 Rb. sphaeroides growth

Reaction centers from carotenoidless mutants (R-26) of *Rb. sphaeroides* were grown and purified for all experiments. The growth medium contained 4 g casamino acid, 40 ml 20 % potassium succinate, 80 ml 1 M phosphate buffer at pH 7, 25 ml 10 % ammonium sulfate, 4 ml vitamin solution as growth factor, and 80 ml metal 44 concentrated base. The final volume was adjusted to 4 liters. The metal 44 concentrated base contains 2 g ethylenediaminetetraacetic acid (EDTA), 11 g zinc sulfate-heptahydrate, 5 g ferrous iron sulfate-heptaphydrate, 1.5 g manganous sulfate-monohydrate, 400 mg cupric sulfate-pentahydrate, 370 mg cobalt chloride-hexahydrate, 120 mg boric acid, and 1.5 ml 6 N sulfuric acid. The final volume was adjusted to 1 liter. All solutions were adjusted to pH 7 with potassium hydroxide of hydrochloric acid and kept at 4 °C (Feher & Okamura 1978).

The growth medium was sterilized for 1 hour using a SV-120 scientific Prevacuum sterilizer and cooled to room temperature. Bacteria were grown under anaerobic conditions. The inoculation of *Rb. spaeroides* from the stock was performed near a Bunsen burner to avoid any contaminations from the air. The inoculated growth medium was put in dark for 5 hours to consume the oxygen inside and then put in the presence of light for 2 days. The cells were centrifuged using Beckman J2-HS centrifuge at 8 000 rpm, 4 °C for 20 minutes. Supernatant was discarded and all the cells were kept at -20 °C (Feher & Okamura 1978).

2.2 Reaction center purification

The reaction center proteins were purified according to Feher & Okamura (1978). 100 g of cells were stirred for 30 minutes in 200 ml distilled water at room temperature. The pH of the solution was kept at 8 using 2 ml 1 M Tris-HCl. After the cells were completely resuspended, 2 ml EDTA was added to chelate metals and 1.25 g NaCl was added to create an ionic strength. The final volume was adjusted to 210 ml after adding 1.7 ml 30 % Lauryldimethylamine-oxide (LDAO). In order to break the cells, 40 minutes of sonication with intervals of 10 seconds was used. After the resuspension and sonication, the cells were centrifuged at 45 000 rpm, 4 °C in Beckman Optima XL-100K Ultracentrifuge for 2 hours in Ti-70 fixed angle rotor at generating a centripetal force equivalent to ~200 000 g times the acceleration of gravity required for chromatophores.

After the first ultracentrifugation, solubilization of the crude BRCs was done by resuspending the pellets in 205 ml TEN (15 mM Tris-HCl, 1 mM EDTA, 0.1 M NaCl) and 4.66 ml 30 % LDAO. The resuspended chromatophores were stirred in the dark at room temperature for 10 minutes. The second ultracentrifugation was also done at 200 000 g, 4 °C for 2 hours in order to form detergent micelles that solubilize the BRCs. The supernatant that contained the crude BRCs was collected and its volume was measured. To isolate the crude BRCs, 30 % ammonium sulfate and 1 % LDAO were used. The crude BRCs were spun at 10 000 rpm, 4 °C for 15 minutes and resuspended in TEN. The resuspended BRCs were dialyzed overnight in $TL^{0.1}E$ (15 mM Tris-HCl, 1 mM EDTA, 0.1 % LDAO) to remove the ammonium sulfate.

Diethylaminoethyl (DEAE) ion exchange chromatography was used for further purification. The DEAE column was pre-equilibriumed with 200 ml $TL^{0.1}E$. After BRCs were loaded onto the column, $TL^{0.1}E$ with a linear salt (NaCl) gradient between 0.03 M and 0.25 M was used to isolate BRCs from other pigments and proteins. The column was cleaned with 1 M NaCl. Protein purity was checked using the ratio of the absorbance at 280 nm and 802 nm (A_{280}/A_{802}), which was kept below 1.8. The absorbance for the aromatic amino acids in BRCs (A_{280}) was known to be 1.2 times the absorbance for bacteriochlorophyll dimer (A_{802}) if BRCs were 100 % pure. The ratio of the absorbance at 760 nm and 865 nm (A_{760}/A_{865}) was kept equal to or lower than 1. BRCs were further concentrated and the concentration was determined from the bacteriochlorophyll dimer absorption band at 802 nm where it had an extinction coefficient ε^{802} of 288 $mM^{-1}\cdot cm^{-1}$ using steady-state absorption spectroscopy (McPherson et al., 1993). The NaCl in the BRCs was removed by 24-hour dialysis using $TL^{0.025}E$ (15 mM Tris-HCl, 1 mM EDTA, 0.025 % LDAO) at 4°C. In order to block the electron transfer from Q_A to Q_B, terbutryn, a potent inhibitor of interquinone electron transfer, was routinely added at a concentration of 100 μM (Kalman et al., 1997). The purified BRCs were all kept at -80 °C.

2.3 Proteoliposome preparation

Liposomes prepared in the present work were from phosphotidylcholines with different fatty acid chains manufactured by Avanti Polar Lipids and were used without further purification (> 99 %). These lipids were all saturated with one exemption. The following four lipids with saturated chains were used: 1,2-Dilauroyl-*sn*-Glycero-3-Phosphocholine (DLPC), 1,2-Dimyristoyl-*sn*-Glycero-3-Phosphocholine (DMPC), 1,2-Dipamytoyl-*sn*-

Glycero-3-Phosphocholine (DPPC), and 1,2-Distearoyl-*sn*-Glycero-3-Phosphocholine (DSPC). These lipids contained fatty acid chains with carbon length of 12, 14, 16 and 18, respectively. The only monounsaturated lipid in this study was 1,2-Dioleoyl-*sn*-Glycero-3-Phosphocholine (DOPC), with 18 carbon length and one double bond at 9^{th} carbon from the head group. All lipids had the same head groups with zero net charge at pH 7.

The reconstitution of BRCs from detergents, in which they were isolated and purified into proteoliposomes was done following the standard procedure (Trotta et al., 2002). 4 mg of Phospholipids were dissolved in 200 µl chloroform in a 1.5 ml Eppendorf tube. The chloroform was slowly evaporated with a continuous nitrogen stream and formed a thin film of phospholipid at the bottom of the tube. The film could be kept at -20 °C for 1 month. The lipid film was dissolved with 0.5 ml of 4 % sodium cholate in phosphate buffer (5 mM, 5 mM KCl, and pH 6-8). The lipid solution was sonicated for 30 minutes to 1 hour with a titanium tip forming lipid-detergent mixed micelles. After the addition of 100 µl concentrated (25 µM) BRC stock solution, the final concentration was adjusted to 4.2 µM with a lipid/protein ratio of 1000:1.

The solution was vortexed at 2500 rpm for 2 minutes to form the detergent/lipid/protein mixed micelles and then loaded on a 15 cm Sephadex G-50 gel filtration column. The column was packed and pre-equilibrated with phosphate buffer at pH 6 to 8. During the elution, the mixed micelles containing BRCs were derived from detergents while the phospholipids and protein could rearrange to form proteoliposomes. The incorporation of BRCs could be inferred by the superposition of a strong background signal due to the

light scattering by the lipid vesicles and an active BRC absorption spectrum (Agostiano et al., 2005).

2.4 Fluorescence polarization measurements

Fluorescence polarization was performed using a Perkin-Elmer MPF-44B fluorescence spectrofluorimeter. A thermostat was used to control the temperature. The temperature was measured inside the cuvette by a low heat capacity portable thermometer. Continuous nitrogen flushing was used at low temperatures to prevent condensation. 1,6-diphenylhexatriene (DPH), which had an excitation at 350 nm and an emission at 430 nm was used as a membrane probe. The emission of DPH was only seen if the molecule is in a hydrophobic environment. In water and other polar solvents, the fluorescence was quenched. DPH was added before loading lipid-detergent mixed micelles on the gel filtration column and the final concentration was adjusted to 16 μM. Linearly polarized light, generated by a polarizing filter, preferentially excited fluorescent target molecules with transition moments aligned parallel to the incident polarization vector. The resultant fluorescence was collected at two orientations of the second polarizer (analyzer): parallel and perpendicular to that of the excitation beam. Fluorescence was measured for DLPC, DMPC, DPPC, and DSPC at multiple temperatures between 0 and 70 °C depending on the lipid. Control experiments were done in tetrahydrofuran (THF) and in detergent Triton X-100.

2.5 Dual polarization interferometry (DPI)

Dual polarization interferometry, as the name suggests, used two polarization angles to

unambiguously determine the thickness of an immobilized macromolecule on a sensor chip by measuring the shifts in the interference pattern generated by illumination with a laser light source. The maximal destructive interference was chosen at the beginning, while depositing a molecule so that the interference pattern generated a positive signal. The thickness of the molecule deposited on the chip surface was calculated accordingly.

The DPI measurement was performed on an Analight Bio200 dual polarization interferometer from Farfield Sienctific Co. The surface used was an unmodified silicon sensor chip, washed with 2 % Hellmanex, 80 % ethanol (w/w) and nanopure water. The temperature of the samples was fixed throughout at 20 °C. All buffers and reagents were dissolved in water of analytical grade or higher, and all solutions were degassed prior to use.

Potassium phosphate buffer (5 mM, 5 mM KCl, pH 7) was delivered at a flow rate of 50 µl/min continuously on the sensor chip. The sensor chip was calibrated with 80 % ethanol and water before loading samples. The lipiposomes collected after the gel filtration column were centrifuged using a 0.22 µm filter to remove large vesicles and were further diluted to 0.2 mg/ml. Liposomes were loaded on the surface of the sensor chip at a flow rate of 12 µl/min.

2.6 Laser flash photolysis (LFP)

Charge recombination reactions were recorded using a miniaturized LPF-112 laser flash photolysis (Luzchem Research) equipped with a pulsed Nd-YAG laser (Continuum, 532

nm output wavelength) as a photoexitation source. Data were collected on a digital storage oscilloscope (Tektronix TDS-2012) in DC-coupled mode. To improve the signal to noise ratio, 20 traces were generated manually with 5-second intervals at monitoring wavelength of 865 nm. Temperature control was performed using a Peltier cell between 4 °C and 45 °C.

2.7 Steady-state absorption spectroscopy

Measurements of charge recombination and conformational rearrangements upon continuous illumination were performed on a Cary 5000 UV-Vis-NIR spectrophotometer from Varian. Temperature control was performed using a Peltier cell between 4 °C and 45 °C. Different illumination intensities were used with nominal output powers ranging from 40 to 250 W using an Oriel tungsten lamp as external illumination source. Spectra were collected from 700 nm to 1000 nm with 0.033 s intergrations and spectral resolution of 0.5 nm. The scan rate was 909 nm/min with full slit height in double beam mode to record the spectra rapidly. Potassium phosphate buffer (5 mM, 5 mM KCl, pH 7) was used as a reference. Baseline was corrected before measuring the spectra. Kinetic traces were recorded in kinetic mode at 865 nm with 0.5 s data interval.

2.8 Data analysis

2.8.1 Fluorescence anisotropy

Fluorescence anisotropy was calculated by the following equation,

$$r = \frac{I_{//} - I_{\perp}}{I_{//} + 2I_{\perp}} \qquad (1)$$

where $I_{//}$ is the fluorescence intensity measured when the confocal planes of the polarizer and analyzer are parallel; $I_{\perp}$ is the fluorescence intensity measured when the confocal planes of the polarizer and analyzer are perpendicular.

2.8.2 Hydrophobic thicknesses of different lipid bilayers

The hydrophobic thickness of a lipid bilayer in the liquid crystalline phase (d_L^f) could be calculated based on the linear function of the acyl chain length (Janiak et al., 1976).

$$d_L^f \cong 1.75(n_c - 1) \text{ [Å]} \qquad (2)$$

where n_c is the number of carbons in the acyl chain. The hydrophobic thickness (d_L^g) is about 30 % larger in the gel phase and has to be corrected by a factor of cos θ, θ being the tilt angle of 30 °, is applied when integral proteins are incorporated into lipid bilayers (Janiak et al., 1976),

$$d_L^g \cong 1.30 d_L^f / \cos 30° \cong 1.50 d_L^f \qquad (3)$$

The mean lipid hydrophobic thickness ($\bar{d}$) was given by as follows (Sperotto & Mouritsen 1988),

$$\bar{d} = \tfrac{1}{2}(d_L^f + d_L^g) \cong 2.19(n_c - 1) \text{ [Å]} \qquad (4)$$

2.8.3 Shifts in the midpoint transition temperature

Phase transition occurred within a temperature range but not at one certain temperature especially with the incorporation of BRCs. Due to the high lipid/protein ratio (1000:1), only a limited amount of lipids near the protein were perturbed by the hydrophobic

mismatch. This produced a heterogeneous population, which broadened the phase transition temperature range. Since there was no mathematical model to fit the lipid phase transition curve, the midpoint phase transition temperature was determined as follows,

Three linear regression lines were fit to the data completely in gel phase, liquid crystalline phase, and temperature ranges during the phase transition, respectively. Another linear regression line was fit to the data of detergent Triton X-100 as a baseline. This baseline was subtracted from the data for the lipids completely in gel phase and liquid crystalline phase. The temperature, at which the midpoint of the regression line fitted to the temperature ranges during the phase transition, was assumed to be the midpoint phase transition temperature (see Fig.8a and 8b in Section *3.1.1*).

Phase transition temperature with the incorporation of BRCs was done in the same way. The shift in the midpoint transition temperature (ΔT) was calculated by subtracting the midpoint transition temperature of the empty liposomes (T_m) from the midpoint transition temperature with incorporated BRCs ($\overline{T}$) (Sperotto & Mouritsen 1988).

$$\Delta T = \overline{T} - T_m \qquad (5)$$

2.8.4 Models to fit shifts in the midpoint transition temperature

Two models were used to fit experimental data depending on the hydrophobic thickness of the lipid bilayer thicker or thinner than the hydrophobic thickness of the BRC.

Laudau-de Gennes theory was used when the hydrophobic thickness of the lipid was thicker than that of the BRC. This model neglected the two-phase coexistence region while only considered a sharp phase transition. The full excess energy was attributed to an elastic distortion, which was proportional to the square of the mismatch (Peschke et al., 1987). The shift in the midpoint transition temperature could be calculated using the following equation,

$$\Delta T = 16\xi^2\left(\frac{Q_p}{\pi\xi}+1\right)\left(\frac{\bar{d}-d_p}{d_L^{0,f}-d_L^{0,g}}\right)x_p \qquad (6)$$

where ξ is the characteristic coherence length of the lipid membrane, within this range from the BRCs, lipids are significantly perturbed by the hydrophobic mismatch; Q_p is the perimeter of the protein section that determines the protein chemical potential; x_p is the protein/lipid ratio; d_p is the hydrophobic thickness of BRC; $\bar{d}$ is the mean lipid bilayer hydrophobic thickness while $d_L^{0,f}$ and $d_L^{0,g}$ are the hydrophobic thicknesses of the lipid bilayers when they are completely in liquid crystalline phase or gel phase, respectively (discussed in Section *2.8.2*).

This type of model had its disadvantage since it could not account for the phase separation. Thus, it was not applicable to fit the data when the hydrophobic thickness of the lipid bilayer was thinner than the hydrophobic thickness of the BRC. Furthermore, the coexistence of the two phases occurred within a large temperature range in DLPC. A two-component solution theory was used in this case. This model considered a linear effect of the hydrophobic matching as well as direct hydrophobic-hydrophobic lipid-protein interactions (Sperotto & Mouritsen 1988). The effect of elastic distortion had

been neglected, which could better explain lipid bilayers with a shorter hydrophobic thickness than that of the BRC. Shift in the midpoint transition temperature was given by,

$$\Delta T(x_p) = \overline{T}(x_p) - T_m \cong \frac{RT_m^2}{\Delta H_L} x_p \sinh(\frac{Qp\Gamma}{RT_m}) \qquad (7)$$

where R is the gas constant; ΔH_L is the transition enthalpy; x_p is the protein/lipid ratio; $Q_p\Gamma$ is the standard chemical potential of the protein; $\overline{T}$ is the midpoint transition temperature with incorporated BRCs while the midpoint transition temperature of the empty liposomes T_m and transition enthalpy ΔH_L can be calculate by the following equations,

$$\Delta H_L[kcal/mole] \cong 0.59\overline{d} - 9.52 \qquad (8)$$

$$T_m[K] = \frac{-1262}{n_c - 3} + 412 = \frac{-1262}{\overline{d}/2.19 - 2} + 412 \qquad (9)$$

where $\overline{d}$ used in equation (8) and (9) is in Å. This model was limited and could not describe the data for cases when the hydrophobic thickness of the lipid bilayers was significantly thicker than that of the protein.

2.8.5 Analyzing the kinetics of charge recombination

The charge recombination kinetics using LFP and steady-state absorption spectroscopy were anaylazed using exponential decays. A mono exponential fit was used when no conformational rearrangements occurred. Two exponentials for the rate constants (k_1, k_2) plus a constant A_0 were used if BRC changed its conformation. Time constants (τ_1, τ_2) were the multiplicative inverse of rate constant (k_1, k_2),

$$A(t) = A_1 e^{-k_1 t} + A_2 e^{-k_2 t} + A_0 \qquad (10)$$

$$\tau_1 = 1/k_1,\ \tau_2 = 1/k_2 \qquad (11)$$

Temperature dependence of the electron transfer reactions was analyzed using Arrhenius Equation,

$$\ln(k) = -\frac{E_a}{R}\cdot\frac{1}{T} + \ln(A_0) \qquad (12)$$

where k is the rate constant; E_a is activation energy; R is the gas constant; T is the absolute temperature; A_0 is a constant.

When a reaction has a rate constant that obeys the Arrhenius equation, a plot of $\ln(k)$ versus $1/T$ gives a straight line, whose slope can be used to determine E_a,

$$E_a(J\cdot mol^{-1}) \equiv -R(\frac{\partial \ln k}{\partial(1/T)}) \qquad (13)$$

3 Results

3.1 Compensation for hydrophobic mismatch from the lipid

Compensation for the hydrophobic mismatch from the lipid was studied by determining the lipid phase transition temperature. The hydrophobic mismatch resulted in different shifts in the midpoint transition temperature towards different directions and extents depending on the lipid hydrophobic thicknesses. Dual polarization interferometry was used to confirm the formation of uni-lamellar liposomes.

3.1.1 Shifts in the midpoint transition temperature with incorporated BRCs

Lipid response to compensate for the hydrophobic mismatch was studied by the phase behavior using fluorescence polarization spectroscopy. Fluorescence anisotropy (r) changes due to the change in membrane fluidity as it was indicated in the lipid phase transition curves of the empty DSPC liposomes and DSPC with incorporated BRCs are shown in Figure 8a. Phase transitions of four different phospholipids with different acyl chain lengths but the same overall neutral head group were measured and data are summarized in Table 1. Control experiments were done with THF and TLE. In THF, a low-viscosity organic solvent, the value for r was zero at all temperatures, which indicated that the system was completely fluidic and DPH could freely rotate. In TLE detergent, the value for r was approaching zero with slight inverse temperature dependence For example from a value of 0.03 at 50 °C, it increased to 0.10 at 5 °C without any steep change indicating that there was no phase transition (Fig.8a). Control experiments demonstrated that in a hydrophobic environment, that did not have a phase

transition, the value for r still increased slowly as temperature decreased with a slope of -0.0013 1/°C.

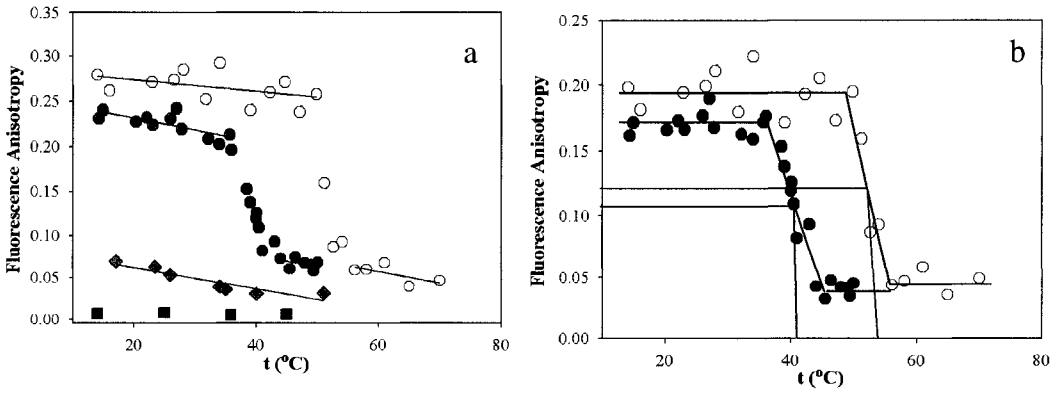

Figure 8. Temperature dependence of fluorescence anisotropy in empty DSPC liposomes (empty circles), DSPC with 4.2 μM BRC (filled circles), THF (squares), TLE detergent (diamonds) using DPH as a membrane probe. Fluorescence anisotropy was fitted with linear regression lines in gel phase, liquid crystalline phase and temperature ranges during the phase transition, respectively. The fitting for TLE detergent was used as a baseline and subtracted from the temperature ranges where DSPC were completely in gel phase and liquid crystalline phase, respectively. (a) Measured data (b) Corrected and fitted data. The cross points of the horizontal lines with an r value of 0.12 (green) for the empty DSPC liposomes and 0.11 (red) for DSPC with incorporated BRCs that passed the midpoint of the regression lines fitted to the temperature ranges during the phase transition were assumed to be the midpoint phase transition temperatures: 53.2 °C for the empty DLPC liposome and 40.7 °C for DLPC with incorporated BRCs. The estimated errors for the midpoint phase transition temperatures are ± 2.0 °C.

At temperatures below 51 °C and above 55 °C in the case of empty DSPC liposomes, the value for r had comparable slopes with the slope determined in detergent micelles (Fig.8a). The linear regression fitting for TLE detergent was used as a baseline and was subtracted from the temperature ranges where liposomes were completely in gel phase and liquid crystalline phase, respectively. The corrected curve is shown in Figure 8b. The

value for r was 0.05 at temperatures above 55 °C and increased to 0.22 at temperatures below 51 °C. At temperatures between 54 °C and 50 °C, a transition from the fluidic liquid crystalline phase to the closely-packed gel phase gave rise to rapid r changes as temperature decreased. This temperature range was assumed to be the width for lipid phase transition. The midpoint phase transition ($\overline{T}$) for empty DSPC liposomes was determined as 53.2 °C with a width of 4 °C (method explained in Section *2.8.3*). With incorporated BRCs, the value for r was around 0.06 at temperatures above 43 °C and increased to 0.17 at temperatures below 37 °C. The midpoint phase transition for DSPC with incorporated BRCs was found to be at 40.7 °C, which was 12.5 °C lower than in the empty liposomes. Reconstitution of BRCs into DSPC liposomes also broadened the transition width by up to 6 °C. This broadening effect was as a result of the heterogeneous population of lipids generated by hydrophobic mismatch. The incorporated BRCs could only influence the lipids within a certain range (defined as coherence length, discussed in Section *2.8.4*) in response to the hydrophobic mismatch. Thus the lipid phase transition with incorporated BRCs was a combination of two different populations: lipids within the coherence length that were perturbed by the hydrophobic mismatch and lipids far away that were not influenced by the hydrophobic mismatch at all.

The same measurements were performed in the other three liposomes and data are summarized in Table 1. In DPPC liposomes, phase transition occurred at 37.8 °C and decreased with the incorporation of BRCs to 33.7 °C with a width of 7 °C. In DMPC liposomes, phase transition occurred at 23.3 °C with a width of 4 °C and decreased with

the incorporation of BRCs to 21.6 °C with a width of 8 °C. Phase transition of DLPC liposomes was not as steep as other lipids. However, since the value for r (before correction) was 0.05 at liquid crystalline phase and 0.30 at gel phase in the rest of the three liposomes, we assumed the same case in DLPC. Phase transition of the empty DLPC liposomes occurred at 0.9 °C with a width of 15 °C and increased with the incorporation of BRCs to 7.3 °C with the same width. The estimated errors for the midpoint phase transition temperatures are ± 2.0 °C. Results were in good agreement with reported values using light scattering methods (Riegier & Mohwald 1986), proving that fluorescence polarization was a suitable method to determine lipid phase transition temperatures.

Lipid	Numbers of carbons in the acyl chain	[1]Acyl chain length (Å)	[2]$\overline{T}$ (°C)	[3]T_m (°C)	[4]ΔT (°C)
DSPC	18	37.2	40.7	53.2	-12.5
DPPC	16	32.9	33.7	37.8	-4.1
DMPC	14	28.5	21.6	23.3	-1.7
DLPC	12	24.1	7.3	0.9	6.4

Table 1. Hydrophobic thicknesses, midpoint phase transition temperatures with and without BRCs and shifts in the midpoint transition temperature of saturated phospholipids with different number of carbons in the acyl chain.

[1]Acyl chain length, which is the hydrophobic thickness of lipid bilayers, linearly increases with the number of carbons in the chain (calculated using Eqs.2, 3, 4). The estimated errors are ± 1.5 Å.

[2,3] $\overline{T}$ and T_m were the midpoint transition temperature with and without BRCs, respectively. The determination of $\overline{T}$ and T_m was explained in Section 2.8.3 and demonstrated in Figure 8. The estimated errors for the midpoint phase transition temperatures are ± 2.0 °C.

[4] ΔT is the shift in the midpoint transition temperature (calculated using Eq.5).

Table 1 summarizes the hydrophobic thicknesses of saturated phospholipids with different fatty acid chain lengths (calculated using Eqs.2, 3, 4), the midpoint transition temperature for both empty liposomes and liposomes with incorporated BRCs, and shifts in the midpoint transition temperature (calculated using Eq.5). The shift in the midpoint transition temperature (ΔT) is defined as the differences between the lipid midpoint phase transition temperature in liposomes with incorporated BRCs ($\overline{T}$) and that of the empty lisposome (T_m). Shifts of −12.5, −4.1, −1.7, and +6.4 °C in the midpoint transition temperature were calculated in DSPC, DPPC, DMPC, and DLPC, respectively. The estimated errors for the shifts in the midpoint phase transition temperatures are ± 2.0 °C. The negative sign represents a downward shift upon incorporating the BRC protein, while the positive sign corresponds to an upward shift in temperature. These results indicate that the direction and extent of the shifts in the midpoint transition temperature are very sensitive to the hydrophobic thickness differences between the lipid bilayers and the protein.

The relationship between the hydrophobic thickness of the lipid bilayer in the liposomes and the shift in the midpoint transition temperature is shown in Figure 9. In lipid bilayers with acyl chains more than 14 carbons, the incorporation of BRC decreases the midpoint transition temperature. The extent of the shift increases as the hydrophobic thickness of the lipid bilayer in the liposomes increases. In DLPC liposomes, BRC reconstitution increases the midpoint transition temperature by 6.4 ± 2.0 °C. Two models are used to fit experimental data corresponding to these two conditions. Laudau-de Gennes theory (theory explained in Section *2.8.4*) is used when ΔT was negative (blue line in Fig.9).

This particular model has a disadvantage namely it cannot account for the phase separation. Phase separation is defined as the conversion of a single-phase system into a multi-phase system, for example, the separation of a solution into two immiscible liquids. It can only be applied if the hydrophobic thickness of the lipid bilayer from the liposome is thicker than that of the protein.

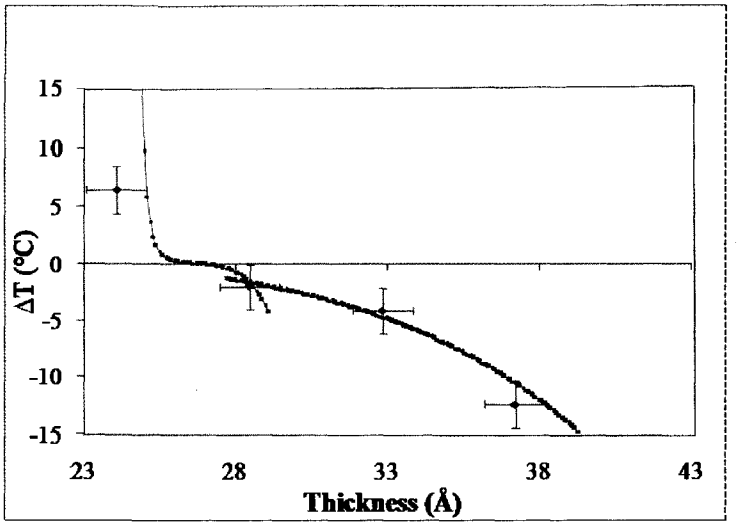

Figure 9. Shift in the midpoint transition temperature (ΔT) as a function of average lipid hydrophobic thickness ($\bar{d}$) in a series of liposomes from saturated phospholipids where the incorporation of the reaction centers has been accomplished.

Conditions: lipid protein ratio = 1000:1, the shift in the midpoint transition temperature was determined at zero ΔT with an average lipid hydrophobic thickness of 26.0 ± 1.5 Å. The blue and red lines represent the fits to Eq.6 and Eq.7, respectively.

The coexistence of the two phases was observed to occur within a large temperature range, 15 °C in DLPC liposomes. Thus, for lipid bilayers from the liposomes with a hydrophobic thickness shorter than that of the BRC, a two-component solution theory (red line in Fig.9, theory explained in Section *2.8.4*) should be used.

Both experimental data and theoretical fits demonstrate that at a hydrophobic thickness of 26.0 ± 1.5 Å, the midpoint transition temperature should not change with the incorporation of BRCs. Liposomes formed from lipids with the optimal value of the hydrophobic thickness eliminate the hydrophobic mismatch upon incorporation of BRCs. A close to optimal thickness was found for bilayers of DMPC liposomes, with a 14 carbon acyl chain length, where the change of the midpoint transition temperature was calculated as -1.7 ± 2.0 °C upon the incorporation of BRCs.

3.1.2 Lipid bilayer thickness determination

To make sure that a uni-lamellar lipisome was formed, dual polarization interferometry (DPI) was used to determine the total thickness of the lipid bilayer.

Figure 10 shows the time course of the deposition of 0.2 mg/ml DLPC on a sensor chip at pH 7 and 20 °C. After 16 minutes of immobilization of DLPC liposomes on the surface of the sensor chip, the thickness gradually increased to 33 ± 1 Å. The thickness kept at 31 ± 1 Å 20 minutes after the deposition finished when all the liposomes that did not bind were washed away from the surface by the running buffer.

Anisotropy effect, defined as the state or quality of having different properties along different axes of the Cartesian coordinate system, is widely seen in natural membranes. This effect was observed in our measurements where the distributions of liposomes were not homogeneous on the chip surface. Liposomes could be compressed and further ruptured into bilayers at a low surface coverage. The thickness could still decrease by

tilting of the lipid bilayers and to a final state of free lipids lying down on the chip surface. Thus the thickness determined was strongly dependent on the surface coverage and density.

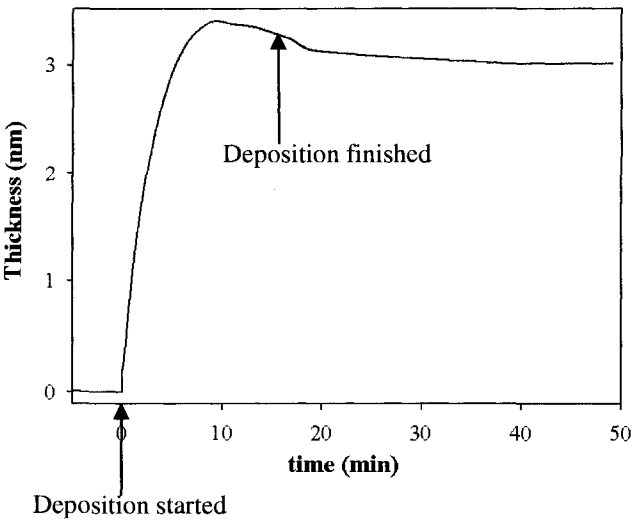

Figure 10. Time course of DLPC deposition. The real time DPI data were collected associated with the deposition of 0.2 mg/ml DLPC liposomes on the sensor chip surface at pH 7, 20 °C starting from time zero. Deposition finished at 16 minutes. All liposomes that did not bind to the surface were washed away by the running buffer (5mM phosphate buffer, 5mM KCl in nanopure water) 20 minutes after the deposition finished.

The thickness of 31 ± 1 Å as we measured was a reasonable thickness for a DLPC lipid bilayer, with a tilting angle around 30°, similar as reported by Sun et al., (1996) and Belgavy et al., (2001).

3.2 Compensation for hydrophobic mismatch from the protein

Protein response to the hydrophobic mismatch was studied by $P^+Q_A^- \rightarrow PQ_A$ electron transfer reaction. The different properties in the absorption spectra at 865 nm in the near

infrared region between P^+ and P have been well characterized and applied to the study of electron transfer reactions in the BRC. In this project, a series of environmental conditions such as the hydrophobic thickness of lipid bilayers, pH, temperature, and illumination conditions that could significantly influence the lifetime of P^+ were changed systematically to study the protein response to the hydrophobic mismatch.

3.2.1 Near-IR absorption spectra of BRC

Due to high conjugation levels, cofactors in BRC have more than one dipole moment: Q_x in the visible region and Q_y in the near-IR region. The solid curve in Figure 11 shows the typical ground state absorption spectrum in the near-IR region. The three absorption bands at 760 nm, 802 nm and 865 nm are attributed to bacteriopheophytins, bacteriochlorophyll monomers, and bacteriochlorophyll dimer, respectively. The bacteriochlorophyll dimer (P) band at 865 nm is bleached (dashed curve in Figure 11) when it gets oxidized, for example, in the presence of light. Permanent dipole-induced dipole interactions induce a hypsochromic shift in the monomer band and a bathochromic shift in the bacteriopheophytin band (Fig.11). The kinetic behavior at 865 nm is well established to study the electron transfer rate of the P^+ formation and recovery.

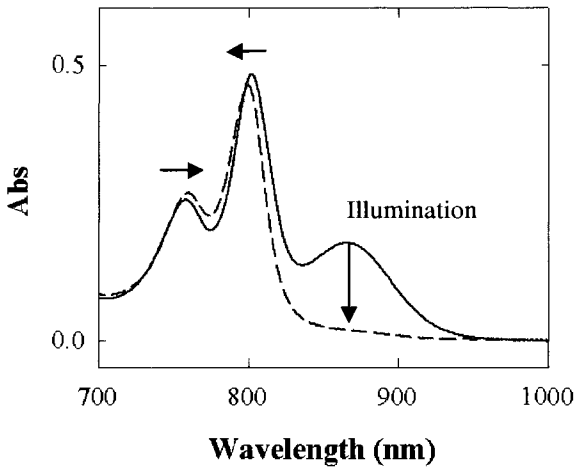

Figure 11. Near-IR absorption spectra of BRC. The solid curve is the ground state spectrum measured in the dark; the dashed curve is the charge separated state spectrum in the presence of light when P gets oxidized to P^+. The bleaching of the P band at 865 nm is accompanied by a hypsochromic shift of the monomer band at 802 nm and a bathochromic shift of the bacteriopheophytin band at 760 nm.

3.2.2 Flash induced $P^+Q_A^- \rightarrow PQ_A$ charge recombination kinetics

The charge separation from Q_A^- to Q_B takes place within ~150 μs (Kleinfeld et al., 1984a). This process can be blocked when inhibitors, such as terbutryn, are bound to BRCs. Under these conditions, the electron is stable in the Q_A^- state until it recombines with P^+ with a lifetime of ~100 ms in wild-type RCs in detergent environments using flash excitations. The lifetime of the $P^+Q_A^-$ can be altered by changing the environmental factors, such as in different liposomes and at different temperatures.

3.2.2.1 Comparison of lipid and detergent environments

Figure 12 shows the kinetic traces of the charge recombination from $P^+Q_A^-$ state to PQ_A state in different environments at room temperature, neutral pH. The traces measured in

liposomes were very similar while differed considerably in detergent. The charge recombination kinetics was well characterized with a single exponential fit in all three cases, resulting in different values of times constants (calculated using Eqs.10, 11): 43 ± 3 ms in DLPC liposomes, 51 ± 4 ms in DMPC liposomes, and 95 ± 6 ms in LDAO detergent micelles. The mono-phasic behavior indicated that upon flash excitations, the recovery of P^+ was a one-step charge recombination process. The lifetime of the $P^+Q_A^-$ charge separated state in liposomes was about half as it was measured in detergent micelles.

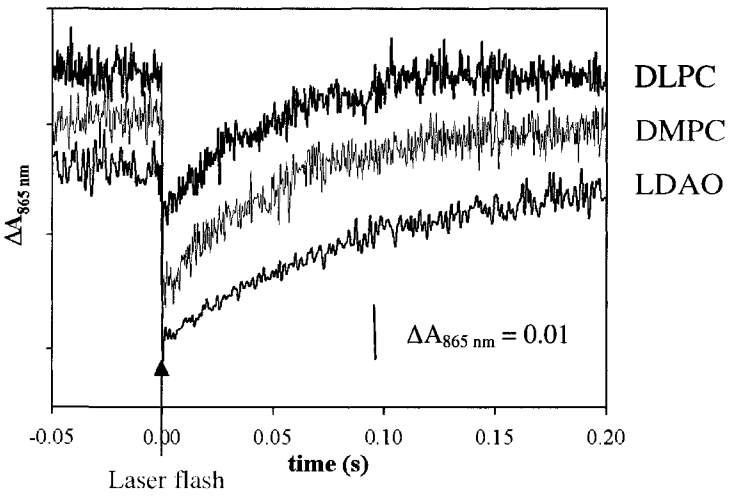

Figure 12. Kinetic traces of flash-induced $P^+Q_A^- \rightarrow PQ_A$ charge recombination reactions recorded in DLPC (black), DMPC (red) liposomes and LDAO (blue) detergent micelles at pH 7, room temperature. In order to block the electron transfer from Q_A^- to Q_B, 100 μM terbutryn was added to 3 μM BRCs. A 5 ns laser flash was given at zero time in the time scale with 5 s intervals. The kinetic traces were well characterized with single exponential fits. The fittings resulted in the following time constants: 42 ± 3 ms, 51 ± 4 ms, 95 ± 6 ms for DLPC, DMPC liposomes, and for LDAO detergent micelles, respectively (calculated using Eqs.10, 11). Kinetic traces were measured at 865 nm and the offset in the figure was vertically separated by OD 0.01 for clarity.

3.2.2.2 Temperature dependence of $P^+Q_A^-$ → PQ_A charge recombination kinetics

The activation energy required for the electron transfer reaction in liposomes was determined by measuring temperature dependence of the $P^+Q_A^-$ charge recombination rate. In DLPC and DMPC liposomes, $P^+Q_A^-$ → PQ_A charge recombination showed only a slight dependence on the temperature, but a strong dependence was observed in LDAO detergent (Fig.13). In LDAO detergent, the value for τ was 105 ± 8 ms at 12 °C and 50 ± 4 ms at 43 °C, which gave an activation energy of 24.9 ± 7.9 kJ·mol^{-1} (calculated using Eqs.12, 13). In DLPC liposomes, the value for τ was 46 ms at 12 °C and 35 ms at 35 °C, which gave an activation energy of 5.9 ± 1.6 kJ·mol^{-1}. In DMPC liposomes, the value for τ was 52 ± 4 ms at 12 °C and 41 ± 3 ms at 45 °C, which gave an activation energy of 4.3 ± 1.4 kJ·mol^{-1}.

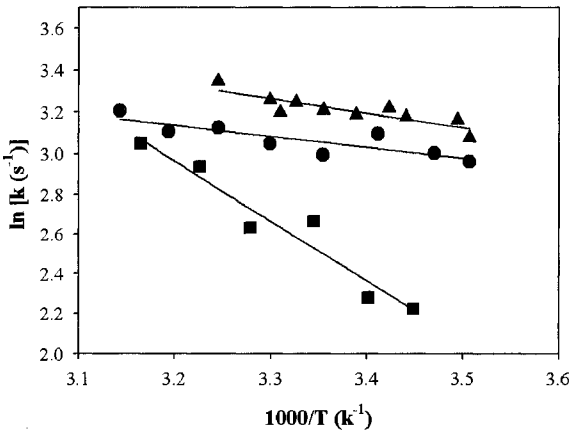

Figure 13. Temperature dependence of the rate constants of flash-induced $P^+Q_A^-$ → PQ_A charge recombination in DLPC (black triangle), DMPC (red circle) liposomes, and in LDAO (blue squares) detergent between 12 °C and 45 °C. From the slopes of Arrhenius plots, the following activation energies were calculated: 5.9 ± 1.6 kJ·mol^{-1} and 4.3 ±1 .4 kJ·mol^{-1}, and 24.9 ± 7.9 kJ·mol^{-1} for the charge recombination reaction in DLPC and DMPC liposomes, and LDAO detergent, respectively (Eqs.12, 13). Conditions as in Figure 12.

The phase transition occurred at 21.6 °C in DMPC liposomes with incorporated BRCs. However, there was no pronounced activation energy difference in the liquid crystalline phase and gel phase in DMPC liposomes.

3.2.3 Conformational rearrangements under continuous illumination

Upon continuous illumination, a long-lived charge separated state was generated with a lifetime of several minutes (Mourik et al., 2001). A similar stabilizing effect of the charge separated state was reported in proteoliposomes of negatively charged phospholipids (Agostiano et al., 2005). The long-lived charge separated state was attributed to an altered light-adapted conformation generated by continuous illumination. The lifetime of the altered light-adapted state was very sensitive to different hydrophobic environments, pH, temperature, and illumination conditions.

3.2.3.1 Comparison of lipid and detergent environments

Figure 14 compares the formation and the recovery of P^+ in LDAO detergent and in DMPC liposomes using 4 minutes of continuous illumination. In both cases, after the illumination was turned on, an unresolved fast kinetic phase was observed, followed by slower phases with lifetimes of several minutes. The fast phase was attributed to the charge separation from the ground state PQ_A to the initial charge separated state $P^+Q_A^-$. The slow and the very slow components were different stages of a conformational rearrangement from a dark-adapted conformation to a light-adapted conformation. The

light-adapted conformation had a much longer lifetime than the dark-adapted conformation since the conformational rearrangement was the rate limiting step.

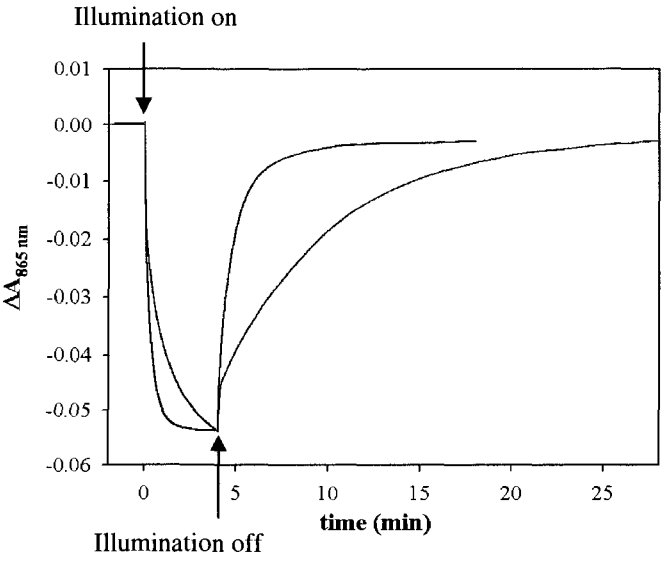

Figure 14. The formation and the recovery of the oxidized dimer P^+ followed by 4 minutes of illumination in LDAO (blue) detergent and DMPC (red) liposomes. Traces were collected in the presence of 1.0 μM BRC with 100 μM terbutryn, 5 mM phosphate buffer with 5 mM KCl at pH 6, at 865 nm, and room temperature. Illumination was turned on at time zero and off at 4 minutes in the time scale. Traces shown were normalized to the same amplitude that recorded just before the illumination was turned off. The kinetic traces were fitted to biexponential decays, with time constants were 37 ± 4 s, 133 ± 11 s for LDAO detergent, and 115 ± 8 s, 357 ± 26 s for DMPC liposomes (calculated using Eqs.10, 11).

When the light was turned off, the recovery of P^+ was also multiphasic with an unresolved fast phase followed by slower reductions of P^+: a slow phase and a very slow phase. By using the biexponential fits, the time constants were determined as 37 ± 4 s, 133 ± 11 s in LDAO detergent and 115 ± 8 s, 357 ± 26 s in DMPC liposomes. These two phases did not involve electron transfer between Q_A and Q_B, which was eliminated by the presence of terbutryn. The kinetic behavior of BRCs both in detergent and liposomes could be repeated several times using subsequent illuminations with the same sample

once P^+ was completely recovered. The amplitude of the very slow component was 26% in LDAO detergent and 50% in DMPC liposome.

The increases in both lifetime and amplitude of the very slow component indicated that the lipid environment facilitated the formation of the long-lived charge separated state. This long-lived charge separated state had a lifetime of 357 ± 26 s in DMPC liposomes at pH 6, which was about three thousand times longer than the lifetime of $P^+Q_A^-$ state induced by flash excitation in LDAO detergent.

3.2.3.2 Lifetime of the long-lived charge separated state at different pH values

The formation and recovery of P^+ were measured over a restricted pH range from 6 to 8. This was due to the fact that during the incorporation of BRCs into liposomes, the size exclusion chromatography method was not completely reliable if the column was operated at pH far from neutrality (Agostiano et al., 2005). A wider pH range could be applied after the liposomes were formed by changing the solution pH and allowing the liposomes to equilibrate.

The values for time constants of the very slow component (τ_2) in three different liposomes are shown in Figure 15 from pH 6 to 8, and they decreased in all three liposomes as pH was increased: 400 ± 32 s to 66 ± 5 s in DLPC liposomes, 303 ± 27 s to 108 ± 10 s in DMPC liposomes, 232 ± 18 s to 108 ± 10 s in DPPC liposomes from pH 6 to 8. These results demonstrat that acidic pH prolongs the lifetime of the light-adapted charge separated state. This could be coupled with a proton release process (Kalman & Maroti 1997), which was also a response to the switch in conformations.

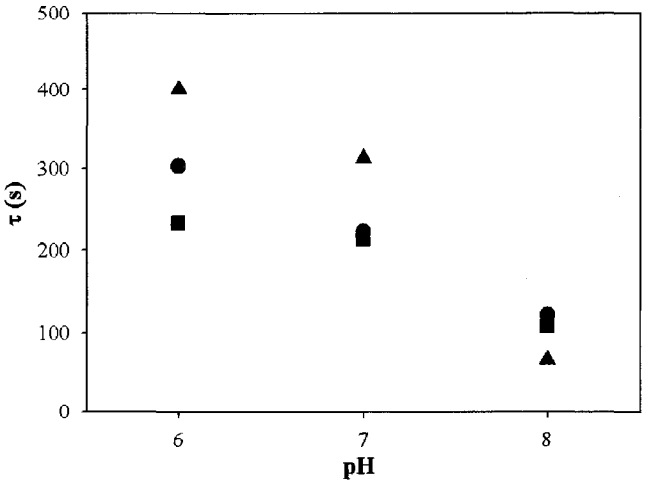

Figure 15. Time constants of the very slow component for the oxidized dimer P^+ recovery in DLPC (black triangles), DMPC (red circles), and DPPC (green squares) liposomes as a function of pH. All measurements were performed using 1μM BRC in 5 mM phosphate buffer (pH from 6 to 8) with 5 mM KCl, 100 μM terbutryn, and 5 minutes of illumination. The value for τ_2 (calculated using Eqs.10, 11) decreased in all three lipids as pH increased.

3.2.3.3 Illumination time dependence of the long-lived charge separated state

The formation of the long-lived charge separated state was reported to be dependent on illumination time (Kalman & Maroti 1997). Even though the long-lived charge separated state upon minutes of continuous illumination had a lifetime about three thousand times as much as the lifetime of $P^+Q_A^-$ state induced by laser flashes, it could be further increased with longer duration of excitations accompanied by a significant increase in the amplitude.

The kinetics traces for the formation and the recovery of the oxidized P^+ in DLPC liposomes using 10 to 60 minutes illumination are shown in Figure 16. The very slow component using 10 minutes of illumination had a time constant of 813 ± 67 s, taking up

27 % of the total amplitude. The amplitude increased to 70 % accompanied by a longer lifetime of 4000 ± 320 s when the illumination was prolonged to 60 minutes. This indicated that 70 % of the BRCs could be generated at the light-adapted charge separated state with a lifetime of 4000 ± 320 s upon 60 minutes of continuous illumination at room temperature.

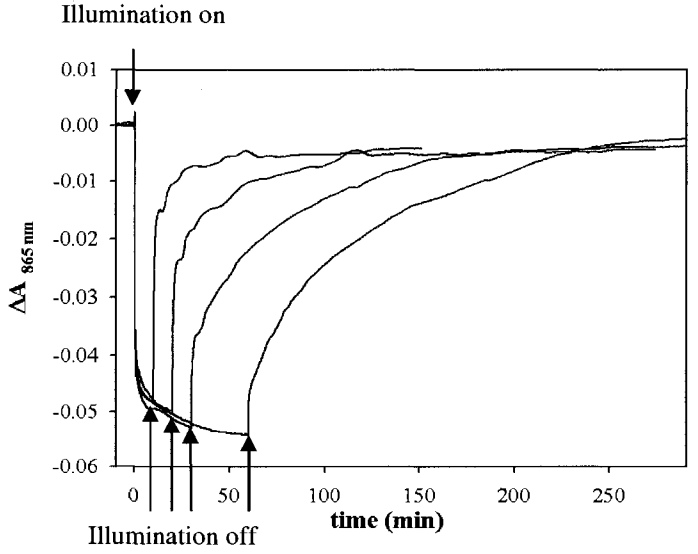

Figure 16. The formation and the recovery of oxidized dimer P^+ in DLPC liposomes with 10, 20, 30 and 60 minutes duration of illumination. Traces were collected in the presence of 1.0 μM BRC with 100 μM terbutryn, 5 mM phosphate buffer with 5 mM KCl at 865 nm, at pH 7 and room temperature. Illumination was turned on at time zero in the time scale and turned off at 10 to 60 minutes, respectively. For the very slow component, the values of the rate constants were 813 ± 67 s, 2040 ± 120 s, 3355 ± 275 s, and 4000 ± 320 s; the amplitudes were determined as 27 %, 39 %, 64%, and 70 % with a illumination time of 10, 20, 30, and 60 minutes, respectively.

3.2.3.4 Temperature dependence of the long-lived charge separated state

Temperature dependence with prolonged illumination was measured to determine the activation energy of the electron transfer reaction as well as the lifetime of the long-lived charge separated state at different temperatures. It was critical to choose a proper

illumination time since it had a significant effect on the lifetime and the amplitude of the long-lived charge separated state. At each and every temperature, saturating illuminations were used to avoid hysteresis. For example, if we illuminated BRCs for 90 minutes above 40 °C, it would degrade and lose its ability to generate the long-lived charge separated state.

Temperature dependences of the very slow kinetic component using saturating illuminations in three different lipids were shown in Figure 17a. Similar to the observations of flash-induced charge recombination reactions, no breaking point was found during the lipid phase transition, for example, 21.6 °C for DMPC liposomes. The activation energy was calculated as 121 ± 20 $kJ \cdot mol^{-1}$ for DLPC, 103 ± 17 $kJ \cdot mol^{-1}$ for DMPC and 67 ± 8 $kJ \cdot mol^{-1}$ for DOPC liposomes, respectively (Eqs.12, 13). The activation energy for LDAO detergent was calculated as 39 ± 5 $kJ \cdot mol^{-1}$.

In DPPC liposomes, the P^+ recovery was even longer than DMPC and DLPC liposomes above 35 °C upon saturating illumination (data not shown), but we were not able to collect any data in the gel phase at this stage due to a large scattering effect.

The kinetic behavior of P^+ formation and recovery in DLPC at 8 °C is shown is Figure 17b using two different types of measurements. The solid line was the kinetic trace collected and the values for τ are calculated as 0.4 ± 0.1 hour and 8.9 ± 0.6 hours with this kinetic method. Circles were collected by taking ΔA_{865} from the spectra recorded at different times during and after illumination. Spectra were corrected by subtracting

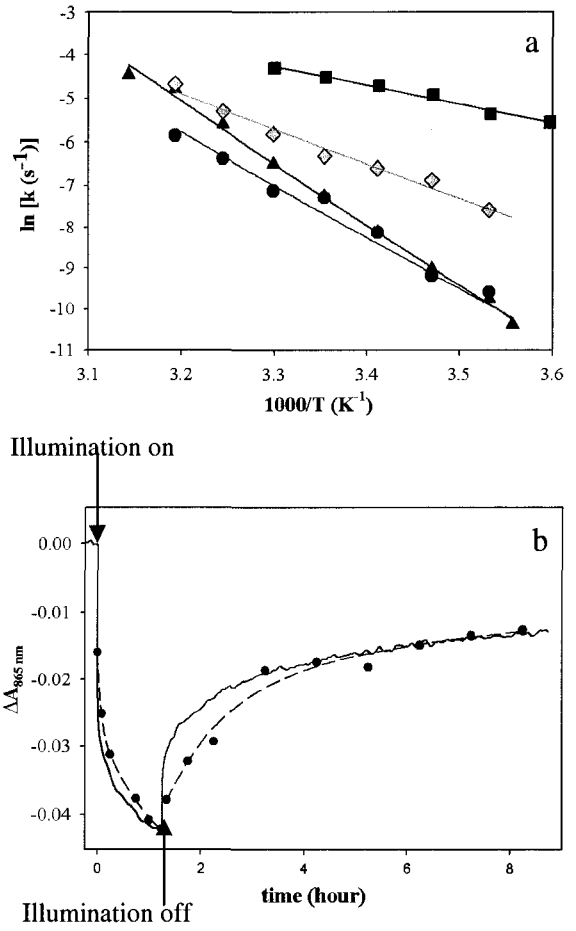

Figure 17. Temperature dependence of the recovery from P^+ for the very slow kinetic component using saturating illuminations (a) in DLPC (black triangle), DMPC (red circle), DOPC (gray diamond) liposomes, and LDAO detergent (blue squares). From the slopes of Arrhenius plots, the following activation energies were calculated: 127 ± 20 kJ·mol^{-1}, 103 ± 17 kJ·mol^{-1}, 67 ± 8 kJ·mol^{-1} and 39 ± 5 kJ·mol^{-1} for DLPC, DMPC and DOPC liposomes, and LDAO detergent respectively (calculated using Eqs.12, 13). (b) The formation and recovery of the oxidized dimer P^+ in DLPC liposomes at 8 °C with 90 minutes illumination. The solid line was the kinetic trace collected in the presence of 1.0 μM BRC with 100 μM terbutryn, 5 mM phosphate buffer with 5 mM KCl at pH 7 at 865 nm; circles were collected by taking ΔA_{865} from the spectra at different times during and after illumination, and were characterized with biexponential fits (dashed line). The values for the time constants were calculated as 0.4 ± 0.1 hour, 8.9 ± 0.7 hours with the kinetic method, and 1.3 ± 0.2 hours, 8.7 ± 0.6 hours in the spectral mode for the slow and very slow components, respectively.

In DPPC liposomes, the P^+ recovery was even longer than DMPC and DLPC liposomes above 35 °C upon saturating illumination (data not shown), but we were not able to collect any data in the gel phase at this stage due to a large scattering effect.

The kinetic behavior of P^+ formation and recovery in DLPC at 8 °C is shown is Figure 17b using two different types of measurements. The solid line was the kinetic trace collected and the values for τ are calculated as 0.4 ± 0.1 hour and 8.9 ± 0.6 hours with this kinetic method. Circles were collected by taking ΔA_{865} from the spectra recorded at different times during and after illumination. Spectra were corrected by subtracting baselines due to the scattering of DLPC liposomes at 8 °C. Absorption changes from the spectra at 865 nm were characterized with a biexponential fit and the values of τ were calculated as 1.3 ± 0.2 hours 8.7 ± 0.6 hours, respectively. Though the lifetime for the slow component was different, the lifetime for the very slow component was very close: 8.7 ± 0.6 hours from the kinetic method and 8.9 ± 0.7 hours with the spectral method. From these two different measurements, we confirmed that this long-lived charge separated state had a lifetime of 8.9 hour in DLPC liposomes at 8 °C upon 90 minutes of continuous illumination, which was about three million times long than that obtained by flash excitation in LDAO detergent.

4 Discussion

Electron transfer reactions in BRCs are highly sensitive to environmental factors, such as hydrophobic thickness of the liposomes or detergent micelles, protonational states of amino acid side chains determined by the pH, and temperature. These factors induce structural changes with different extents and the generated structural rearrangements alter the energetics of the electron transfer rate. Artificial membranes provide a better approximation than the detergent micelle environment to explore the structure-function relationship of the BRCs because they represent a milieu that closely resembles the conditions *in vivo*. Earlier studies provided evidence that key functional parameters of the electron transfer reaction are significantly different in isolated BRCs than in the natural membrane environment. For example, the lifetime of the $P^+Q_B^-$ charge separated state was very similar in chromatophores and in liposomes, while it was reported by about an order of magnitude shorter in detergent micelles (Trotta et al., 2002, Nagy et al., 2004). By systematically optimizing the membrane environment, our ultimate goal is to develop an artificial membrane system that maximizes the function of the BRC or apply BRCs into man-made devices such as bio-capacitor. In the present work, we studied the influence of the membrane thickness for the electron transfer and the stability of the light-generated conformational states of the reaction center from purple photosynthetic bacterium *Rhodobacter sphaeroides*.

4.1 Factors influencing the electron transfer: Marcus theory

Arguably the most efficient electron transfer processes take place in the reaction center proteins of photosynthetic organisms. The efficiency of the electron transfer characterized by the quantum yield of the charge separation in these complexes is barely distinguishable from unity. This means that each and every absorbed photon triggers a transmembrane electron transfer and no photons are wasted. The initial electron transfer of the charge separation is among the fastest electron transfer processes in Nature transferring an electron over 2 nm distance from the dimer to the bacteriopheophytin in 3 ps time (Allen et al., 1987). Just for a comparison during this 3 ps time interval even the light can only cover 0.6 mm distance. No wonder that the currently accepted electron transfer theory was developed using these photosynthetic processes and brought the recognition in the form of the Nobel Prize in Chemistry to the developer Rudolph Marcus in 1992. According to Marcus electron transfer theory (Marcus & Sutin 1985, Marcus 1992), the rate constant of the electron transfer, k, is given by,

$$k = A\exp\left[\frac{-(\Delta G^{act})^2}{k_B T}\right] = A\exp\left[\frac{-(\lambda + \Delta G^0)^2}{4\lambda k_B T}\right]$$

(14)

Where ΔG^{act} is the activation energy; ΔG° is the free energy difference between the final and initial states, normally negative for an exothermic reaction and positive for an endothermic reaction; λ is the reorganization energy, defined as the energy required to distort the nuclear configuration of the reactants into the nuclear configuration of the products without the electron transfer occurring; A, the pre-exponential factor, is the electronic coupling between the electron donor and acceptor indicating how well the potential energy surfaces of the reactants overlap. This parameter is primarily determined

by the distance between the molecules or groups that donate the electron and the one that accepts it. In practical terms this is the maximum limit for the rate constants if all the other parameters are optimized. In Equation 14, T is the temperature; k_B is the Boltzmann constant. The reorganization energy is very sensitive to even the slightest structural changes as evidenced by the following two equations,

$$\lambda = \lambda_{solv} + \lambda_{vib} \tag{15}$$

Where λ_{solv} is the reorganization energy due to changes in solvent orientation, (here the protein matrix) and λ_{vib} is the reorganization energy due to changes in bond lengths of the reactants (vibrations). λ_{solv} can be further calculated as follows,

$$\lambda_{solv} = \frac{e^2}{2}\left(\frac{1}{\varepsilon_{op}} - \frac{1}{\varepsilon_s}\right)\left(\frac{1}{R_D} + \frac{1}{R_A} - \frac{2}{R_{DA}}\right) \tag{16}$$

where ε_{op} is the optical dielectric constant, better known as refractive index; ε_s is the static dielectric constant, which describes the amount of stored energy when a potential is applied; R_D and R_A are the radii of the two electron donor and acceptor, respectively; and R_{DA} is the center-to-center distance between the electron donor and acceptor. Normally we use relative dielectric constant, simplified as dielectric constant ε, which can be calculated as the ratio of static permittivity of a material, relative to the vacuum permittivity (electric constant ε_0),

$$\varepsilon = \frac{\varepsilon_s}{\varepsilon_0} \tag{17}$$

From the last four equations one can conclude that in order to transfer an electron efficiently in a biological macromolecule, the driving force and the reorganization energy both must be relatively small providing the minimum activation energy. Common sense might suggest that a larger driving force would provide faster electron transfer rate, but

from Figure 18b it is obvious that the optimal value of $-\Delta G^0$ is that equals to the reorganization energy. This match results in activationless process with the maximum possible rate constant. To keep the reorganization energy small the distance between the donor and acceptor (R_{DA}) must be small along with the dielectric constant of the protein environment (ε), and the sizes of the donor and acceptor molecules must be large (Eq. 16). Out of these parameters the environment can affect ΔG^0, λ, and within λ only ε and the R_{DA}.

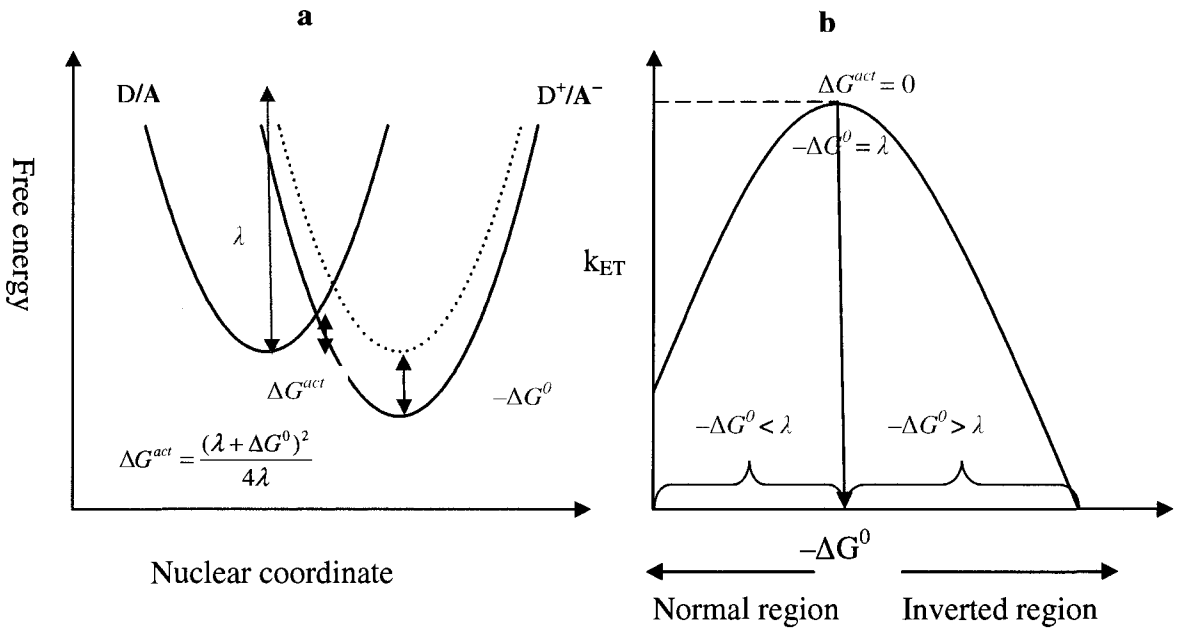

Figure 18. Free energy curves in an electron transfer reaction applied with Marcus theory. (a) Free energy curves of reactants and products as a function of nuclear coordinate. The left solid parabola represents the potential energy surface for the nuclear motion of the reactants in the initial state (D/A), and the right solid parabola represents the potential energy surface for the nuclear motion of the products in the final state (D^+/A^-). Electron transfer has to occur at the crossing point of these two solid parabolas, representing the energy level to which the D/A state must be raised (ΔG^{act}) before progressing to the D^+/A^- state. The reorganization energy (λ) is the energy required to transfer the electron from the bottom of the left solid parabola of the donor at the same nuclear configuration to the right dashed curve of the acceptor.

The driving force is the free energy difference between the initial and the final state, normally negative for an exothermic reaction and positive for an endothermic reaction. (b) Dependence of electron transfer rate upon the free energy difference. In the normal region where the driving force ($-\Delta G^0$) is smaller than the reorganization energy, the electron transfer rate increases as the driving force increases. The rate reaches maximum when the driving force equals to the reorganization energy. In the inverted region where the driving force is larger than the reorganization energy, the electron transfer rate decreases as the driving force increases.

4.2 Change of the driving force in lipid environment upon charge separation

Under physiological circumstances, the $P^+Q_A^- \rightarrow PQ_A$ charge recombination process takes place within 100 ms. It is known that the non-adiabatic electron transfer takes place over a large range of 25 Å. A non-adiabatic electron transfer process is a quantum jump of the electron transfer from one parabola to the other parabola at the crossing point (see Figure 18a). The free energy difference between the initial $P^+Q_A^-$ state and the final PQ_A state ($-\Delta G^0$) was approximately 500 meV in wild-type BRCs. And the reorganization was modeled and reported as 930 meV in wild-type BRCs at room temperature (Ortega et. al 1996).

The lifetime of the $P^+Q_A^-$ charge-separated state could be changed by altering the free energy difference between $P^+Q_A^-$ and PQ_A states, which could be approached by either replacing the ubiquinone Q_A with quinones that had different red-ox potentials (Kalman & Maroti 1994) or designing a series of mutants with different P/P^+ midpoint potentials (Lin et. al 1994). This lead to an altered lifetime of the $P^+Q_A^-$ charge-separated state between 3 ms and 400 ms. Another approach was to decrease the temperature to

cryogenic temperature that significantly decreases the reorganization energy. The lifetime of the $P^+Q_A^-$ state from the wild-type BRC decreased from 100 ms at 293 K to 20 ms at 10 K (Ortega et. al 1996).

Studies above have been carried out in detergent environments. In liposomes composed of phospholipids, a similar lifetime of the $P^+Q_A^-$ charge-separated state of 115 ms in *Rb. sphaeroides* BRCs has been reported (Gopher et. al 1985, Milano et. al 2003). However, the $P^+Q_A^- \rightarrow PQ_A$ charge recombination has been found to be significantly faster in BRCs in *Rhodopseudomonas viridis* in liposomes than in detergent micelles (Sebban & Wraight 1989). Recently, Nagy et al., (2004) reported a significant increase in the energy level of $P^+Q_A^-$, which represented in a larger value of $-\Delta G^0$.

In this project, the lifetime of the $P^+Q_A^-$ charge separated state was measured as 43 ± 3 ms, 51 ± 4 ms and 95 ± 6 ms in DLPC, DMPC liposomes, and in LDAO detergent, respectively, which were significantly faster than the reported values in BRCs from *Rb. sphaeroides* in lipid environments. The monophasic behavior of the P^+ recovery kinetics was very fast, proving that no major conformational rearrangement occurred induced by flash excitations during this electron transfer processes. This suggested that the reorganization energy did not change significantly. With a larger value of $-\Delta G^0$, the activation energy decreased in lipid environment, which resulted in a fast charge recombination rate. Future perspective included the measurement of P/P^+ and Q_A/Q_A^- midpoint potentials of BRCs in liposomes, which would verify that the shorter lifetime was due to the change in the driving force or not.

It was well established that the rate constant of the $P^+Q_A^-\rightarrow PQ_A$ charge recombination reaction increased when the temperature is decreased below 265 K because of the decrease in the reorganization energy. At temperatures above 273 K, the rate constant was almost independent from the temperature suggesting a nuclear tunneling process (Ortega et al., 1996). Recently, a small increase of the rate constant has been reported above 270 K, which was modeled and demonstrated to be as a result of the different hydrogen bonds to quinones in the ground state and the charge separated state (Krasilnikov et al., 2007). In the present work, the rate constant of the $P^+Q_A^-\rightarrow PQ_A$ charge recombination reaction induced by flash excitations increased slowly as temperature increased slowly between 285 K and 318 K in liposomes, but was fast in detergent. The activation energy for the charge recombination reaction was 5.9 ± 1.6 $kJ\cdot mol^{-1}$, 4.3 ± 1.4 $kJ\cdot mol^{-1}$, and 24.9 ± 7.9 $kJ\cdot mol^{-1}$, in DLPC, DMPC liposomes, and in LDAO detergent respectively. The small activation energy in liposomes verified the results that the lifetime of $P^+Q_A^-$ was shorter in liposomes than in detergent due to the change in the driving force.

4.3 Protein conformational rearrangements

Upon continuous illumination, BRC maintained a charge-separated state with a lifetime varying from a few minutes up to 20 minutes in TX-100 and LDAO detergent (Kalman & Maroti 1997, Mourik et. al 2001), chromatophores (Goushcha et al., 2003), and in proteoliposomes of negatively charged phospholipids (Agostiano et al., 2005). They all attributed this as the lifetime of conformationally altered states with long lifetimes

significantly different from charge recombination. The multiphasic kinetic behavior of the oxidized dimer recovery both in LDAO detergent micelles and DMPC liposomes (Fig.14) verified the existence of the long-lived charge separated state. Moreover, the lifetime for the long-lived charge separated state was significantly longer together with larger amplitudes of the kinetic components associated with these conformational rearrangements in liposomes than in detergent micelles. These differences proved that the lipid environment facilitated the formation of the long-lived charge separated state. A minimum model was used to describe the electron transfer process accompanied by the conformational rearrangement (Scheme 1). Different stages could be reached if we used different duration of illumination. The final light adapted state $[P^+Q_A^-]^*$ could only be reached under optimal conditions, for example, with saturation illumination where further illumination did not change the rate constant. The recovery was multiphasic: the fast unresolved component was a direct charge recombination from the dark-adapted charge separated state $[P^+Q_A^-]$ to the ground state $[PQ_A]$; the slow and very slow components were the recovery from different charge separated stages to the ground state $[PQ_A]$, with the conformational rearrangement as the rate limiting step.

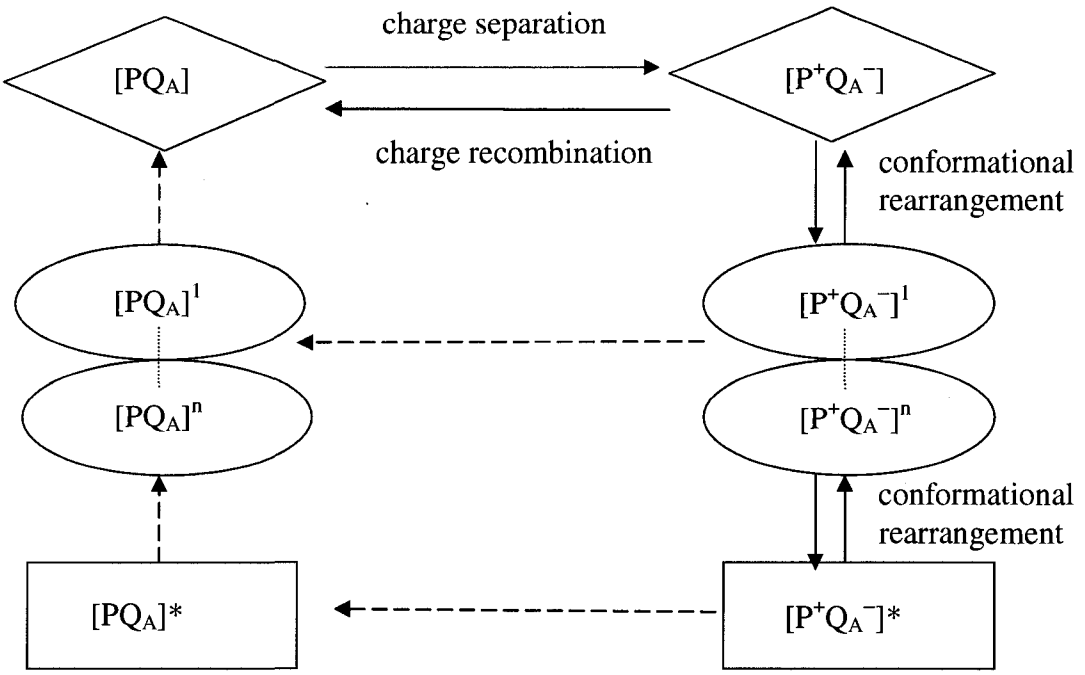

Scheme 1. A minimal model describing the electron transfer process and conformational rearrangements during continuous illumination. Charge separation occur from the ground state $[PQ_A]$ to a dark-adapted charge separated state $[P^+Q_A^-]$ when the illumination is turned on. With continuous illumination, the $[P^+Q_A^-]$ state undergoes conformational rearrangements to several intermediate states $[P^+Q_A^-]^1$ to $[P^+Q_A^-]^n$ and can stop at any stage if the environmental conditions does not allow further rearrangements. The light-adapted state $[P^+Q_A^-]^*$ can be reached under optimal conditions with a certain population, for example long saturated illumination. When the light is turned off, the fast kinetic component is the direct charge recombination from $[P^+Q_A^-]$ state to the ground state $[PQ_A]$. The slow components with different rate constants were attributed to the recovery from different charge separated states to the ground state while the conformational rearrangement is the rate limiting step. Black solid arrows represent reactions under illumination; red solid arrows represent dark reactions; dashed arrows are the processes that are unlikely to happen, and dashed lines are the intermediate stages from 1 to n.

4.4 Change in the reorganization energy upon continuous illumination

The accumulation of the altered light-adapted state was quite natural if we considered the stress invoked on the BRCs by the radical pair, P and Q_A. Mourik et al., (2001) proposed a increase in the value of ε, which caused a significant increase in the reorganization energy during the conformational rearrangement process (Eq.16). With one electron and a hole with a diameter of 25 Å from P^+ to Q_A^-, the attractive force is around 30 pN/ε. This force would correspond to a pressure of 30/ε kbar working on a surface of 1 nm^2, which is sufficient to denature most of the proteins if the dielectric constant was small. For proteins with large hydrophobic regions like the BRC, the dielectric constant is generally thought to be as low as 4. This demonstrates that in the need for BRC for the shielding of the charges, dielectric relaxation should occur. Dielectric relaxation refers to the relaxation response of a dielectric medium to an external electric field. For most modeling calculations, the dielectric constant uses values of ~20. There is no direct evidence that the value of R_{DA} change together with the conformational rearrangement at this stage. This increase in the dielectric constant would raise the reorganization energy, which decreased the electron transfer rate (Eq. 16).

4.5 The stabilization effect of the charge separated state in liposomes

The lifetime of the long-lived charge separated step increased at low pH. This suggested that acidic pH favored the conversion of the BRCs from the dark-adapted state to the light-adapted state. From the electron donor side, Kalman & Maroti (1997) observed a large proton release at the light-adapted conformation at acidic pH. They suggested that the conformational change was controlled by protonatable side chains of the protein. In the light-adapted state, BRC exposed several buried and ligated groups around the

oxidized dimer to the bulk. From the acceptor side, there is no protonatable residue in the 12 Å vicinity of Q_A when it is in the ground state or in the dark-adapted $[P^+Q_A^-]$ state. A different conformation of the Q_A^- was reported by Andreasson et al., (2003) and Agositiano et al., (2005) using electron paramagnetic resonance spectroscopy. They suggested a re-arrangement of the proton network residues surrounding Q_A^- could contribute to the stabilizing of the light-adapted conformation.

It was reported that at low temperatures the long lifetime became even longer with a stronger dependence on the illumination time (Mourik et. al 2001). The longest lifetime we obtained was measured as 8.9 ± 0.7 hours in DLPC liposomes at 8 °C under 90 minutes illumination. We calculated the activation energies as 121 ± 20 $kJ \cdot mol^{-1}$, 103 ± 17 $kJ \cdot mol^{-1}$, 66 ± 8 $kJ \cdot mol^{-1}$ for DLPC, DMPC, and DPPC liposomes respectively. The activation energy measured in LDAO detergent was calculated to be 39 ± 5 $kJ \cdot mol^{-1}$, comparable to the value of 36 ± 4 $kJ \cdot mol^{-1}$ for a quadruple mutant BRC (Kalman et al., 2004). The large value of ΔG^{act} in liposomes also verified the slow recovery of the oxidized dimer.

4.6 Electron transfer influenced by lipid bilayer thickness

The head to head distance that included the both the hydrophobic fatty acid chain and the hydrophilic head group has been studied by Sun et al., (1996) and Belgavy et al., (2001) using low angle scattering methods. The reported value for a DLPC bilayer was calculated to be 34 Å and 36 Å at 20 °C, including the 8–10 Å head groups. If we add the lengths of the head groups and the theoretical hydrophobic thickness for DLPC, the head

to head thickness is assumed to be 32-34 Å, which is in good agreement with the 31 ± 1 Å thickness obtained from the dual polarization interferometry measurement.s

DMPC bilayers have the optimal hydrophobic thickness for the BRCs. The recovery of P^+, as well as the activation energies were very similar in DLPC and DMPC liposomes upon flash excitation. Upon continuous illumination, the activation energies increased significantly in both DLPC and DMPC liposomes, resulting in the long lifetime of the charge separated state. However, the activation energies were still very close in DLPC(121 $kJ \cdot mol^{-1}$) and DLPC (103 $kJ \cdot mol^{-1}$) liposomes, We obtained a faster recovery in liposomes than in detergent induced by laser flashes but a slower recovery in liposomes than in detergent upon continuous illumination, which were in good agreement with the activation energies calculated from the Arrhenius plot. In DOPC, the mono-unsaturated liposomes, the activation energy was about half compared with saturated liposomes upon continuous illumination. However, it was still almost twice as much as it was in detergent environment. This suggested that the lipid environment facilitated the formation of a long-lived light-adapted $[P^+Q_A^-]^*$ state, whose lifetime was limited by the conformational rearrangement process. Future perspectives should also include the study for the saturation level and head group charges influencing the structure and the function of the protein.

4.7 Conclusion

Liposomes with different bilayer hydrophobic thicknesses facilitate the formation of a long-lived charge separated state $[P^+Q_A^-]^*$ upon long saturating illumination. This state is

proved to be an altered light-adapted stated from the dark-adapted state [$P^+Q_A^-$], and the recovery to the ground state is limited by a conformational rearrangement process. Lipid environment, acidic pH, long illumination time, and low temperature favor this conformational change. Although altered conformation has already been proposed, its lifetime could only be raised up to 20 minutes. In this project, by systematically optimizing the environment factors, the charge can be separated for 8.9 hours, which is three million times longer than the lifetime of the charge separated state induced by laser excitation.

References

Agostiano, A., Milano, F. & Trotta, M. (2005) Trapping of a long-living charge separated state of photosynthetic reaction centers in proteoliposomes of negatively charged phospholipids, *Photosynth. Res. 83,* 53 – 61

Allen, J.P., Feher, G., Teastes, T.O., Komiya, H., and Rees, D.C. (1987) Structure of the reaction center from *Rhodobacter sphaeroides* R-26: the cofactors, *Proc. Natl. Acad. Sci. 84*, 5730 – 5735

Andreasson U. & Andreasson L-E. (2003) Characterization of a semi-stable, charge-separated state in reaction center from *Rhodobacter sphaeroides*. *Photosynth. Res. 75*, 223 – 233

Axelrod, H.L. & Okamura, M.Y. (2005) The structure and function of the cytochrome c_2: reaction center electron transfer complex from *Rhodobacter sphaeroides*, *Photosynth. Res. 85*, 101 - 114

Belgavy, P., Dubnickova, M., Kucerka, N., Kiselev, M.A., Yaradaikin, S.P. & Uhrikova. (2001) Bilayer thickness and lipid interface are in unilamellar extruded 1,2-diacylphosphatidylcholine liposomes: a small-angle neutron scattering study, *Biohim. Biophys. Acta. 1512*, 40 – 52

Bowie, J.U. (2005) Solving the membrane protein folding problem, *Nature 438*, 518 – 589

Camara-Artigas, A., Brune, D. & Allen, J.P. (2002) Interactions between lipids and bacterial reaction centers determined by protein crystallography, *Proc. Natl. Acad. Sci. 99*, 11055 – 11600

Feher, G. & Okamura, M.Y. (1978) Chemical composition and properties of reaction centers. In the *Photosynthetic Bacteria*. Clayton, R.K. & Sistrom, W.R. as editors, Plenum Press, New York, 349 – 386

Goushcha, A.O., Manzo, A.J., Scott, G.W., Chrisophorov, L.N., Knox, P.P., Barabash, U., Kapoustina, M.T., Berezetzka, N.M. & Kharkyanen, V.N. (2003) Self-regulation phenomena applied to bacterial reaction centers: 2. Non-equilibrium adiabatic potential: dark and light conformations revisited. *Biophys. J. 84*, 1146 – 1160

Gopher, A., Blatt, Y., Schonfeld, M, Okamura, M.Y. & Feher, G (1985) The effect of an

applied electric field on the charge recombination kinetics in reaction centers reconstituted in planar lipid bilayers, *Biophys. J. 48*, 311– 320

Janiag, M.G., Small, D.M. & Shipley, G.G (1976) Nature of the thermal pretransition of synthetic phospholipids, dimyristoyl and diapamitoyllecithin. *Biochemistry 15*, 4575 – 4580

Kalman, L. & Maroti, P. (1994) Stabilization of reduced primary quinone by proton uptake in reaction centers of *Rhodobacter sphaeroides*, *Biochemistry 33*, 9237 – 9244

Kalman, L., & Maroti, P. (1997) Conformation-activated protonation in reaction centers in the photosynthetic bacterium *Rhodobacter sphaeroides*, *Biochemistry 36*, 15269 – 15276

Kalman, L., Narvaes, A.J., Lobrutto, R., Williams, J.C. & Allen, J.P. (2004) Dependence of tyrosine oxidation in highly oxidizing bacterial reaction centers on pH and free-energy difference, *Biochemistry 43*, 12905 – 12912

Kalman, L., Williams, J.C. & Allen J.P. (2008) Comparison of bacterial reaction centers and photosystem II, *Photosynth. Res.* submitted on June 03, 2008

Ke, B. (2001) *Photosynthesis: photobiochemistry and photobiophysics*, Kluwer Academic Publishers, Dordrecht, Boston

Kleinfeld, D., Okamura, M.Y. & Feher, G. (1984) Electron transfer in reaction centers of *Rhodobacter sphaeroides*. I. Determination of the charge recombination pathway of $D^+Q_AQ^-$ and free energy and kinetic reactions between $Q_A^-Q_B$ and $Q_A\ Q_B^-$, *Biochim. Biophys. Acta 766*, 126 – 140

Kirasilnikov. P.M., Mamonov, P.A., Knox, P.P., Paschenko, V.Z. & Rubin, A.B. (2007) The influence of hydrogen bonds on electron transfer rate in photosynthetic RCs, *Biochim. Biophys. Acta. 1767*, 541 – 549

Marcus, R.A. & Sutin, N. (1985) Electron transfers in chemistry and biology, *Biochim. Biophys. Acta 811*, 265 – 322

Marcus, R.A. (1992) Electron transfer reactions in chemistry: theory and experiment, *Nobel lecture*, December 8, 1992

McPherson, P.H., Okamura, M.Y. & Feher, G. (1993) Light-induced proton uptake by photosynthetic reaction centers from *Rhodobacter sphaeroides* R-26.1 II. Protonation of

the state $DQ_AQ_2^-{}_B$, *Biochim. Biophys. Acta 1144*, 309 – 324

Milano, F., Agositiano, A., Mavelli, F. & Trotta, M. (2003) Kinetics of the quinone binding reaction at the Q_B site of reaction centers from the purple bacteria *Rhodobacter sphaeroides* reconstituted in liposomes, *Eur. J. Biochem. 270*, 4595 – 4605

Mourik, F.V., Reus, M. & Holzwarth, A.R. (2001) Long-lived charge-separated states in bacterial reaction centers isolated from *Rhodobacter sphaeroides*, *Biochim. Biophys. Acta. 1504*, 311 – 318

Muh, F., Rautter, J. & Lubitz, W. (1997) Two distinct conformations of the primary electron donors in reactions centers from *Rhodobacter spaeroides* revealed by ENDOR/TRIPLE-spectroscopy, *Biochemistry 36*, 4155 – 4162

Ortega, J.M., Mathis, P., Williams, C.J. & Allen, J.P. (1996) Temperature dependence of the reorganization energy for charge recombination in the reaction center from *Rhodobacter sphaeroides*, *Biochemistry 35*, 3354 – 3361

Peschke, J., Rieger, J. & Mohwald, H. (1987) Quantitative analysis of membrane distortion induced by mismatch of protein and lipid hydrophobic thickness, *Eur. Biophys. J.* 14, 385 – 391

Riegler, J. & Mohawald, H. (1986) Elastic interactions of photosynthetic reaction center proteins affecting phase transitions and protein distributions, *Biophys. J. 49*, 1111 – 1118

Roth, M., Arnoux, B., Ducriux, A. & Reiss-Husson, F. (1991) Structure of the detergent phase and protein-detergent interactions in crystals of the wild type (Strain Y) *Rhodobacter sphaeroides* photochemical reaction center, *Biochemistry 30*, 9403 – 9413

Sanderson, J.M. (2005) Peptide-lipid interactions: insights and perspectives, *Org. Biomol. Chem. 3*, 201 – 212

Sebban, P. & Wraight. C.A. (1989) Heterogeneity of the $P^+Q_A^-$ recombination kinetics in reaction centers from *Rhodopseudomonas viridis*: the effect of pH and temperature, *Biochim. Biophys. Acta. 974*, 54 – 65

Sperotto, M.M. & Mouritsen O.G. (1988) Dependence of lipid membrane phase transition temperature of the mismatch of protein and lipid hydrophobic thickness, *Eur. Biophys. J. 16*, 1 – 10

Stowell, M.H.B., McPhillipis, T.M., Rees, D.C., Soltis, S.M., Abresch, E. & Feher, G.

(1997) Light-induced structural changes in photosynthetic reaction center: implications for mechanism of electron-transfer, *Science 276*, 812 – 816

Sun, W.J., Tristran-Nagle, S., Suter, R.M. & Nagle, J.F. (1996) Structure of gel phase saturated lecithin bilayers: temperature and chain length dependence, *Biophys. J. 61*, 885 – 891

Trotta, M., Milano, F., Nagy, L. & Agostiano, A. (2002) Response of membrane protein to the environment: the case of photosynthetic reaction center, *Mater. Sci. Eng. C 22*, 263 – 267